International
Progress Report

IPR-03-51

Äspö Hard Rock Laboratory

Long-Term Diffusion Experiment

Structural model of the LTDE site and detailed description of the characteristics of the experimental volume including target structure and intact rock section

Anders Winberg, Conterra AB

Jan Hermanson, Golder Associates AB

Eva-Lena Tullborg, Terralogica AB

Isabelle Staub, Golder Associates AB

November 2003

Svensk Kärnbränslehantering AB
Swedish Nuclear Fuel
and Waste Management Co
Box 5864
SE-102 40 Stockholm Sweden
Tel 08-459 84 00
+46 8 459 84 00
Fax 08-661 57 19
+46 8 661 57 19

Äspö Hard Rock Laboratory

Report no.
IPR-03-51

No.
F79K

Author
Anders Winberg
Jan Hermanson
Eva-Lena Tullborg
Isabelle Staub

Date
Nov 2003

Checked by
Mats Skålberg

Date

Approved
Christer Svemar

Date
2004-10-17

Äspö Hard Rock Laboratory

Long-Term Diffusion Experiment

Structural model of the LTDE site and detailed description of the characteristics of the experimental volume including target structure and intact rock section

Anders Winberg, Conterra AB

Jan Hermanson, Golder Associates AB

Eva-Lena Tullborg, Terralogica AB

Isabelle Staub, Golder Associates AB

November 2003

Keywords: Characterisation, damage, drilling, fracture, LTDE, KA3065A02, KA3065A03, stress, structural model

Abstract

Drilling of an experimental borehole (KA3065A03) for the purpose of the Long-Term Diffusion Experiment (LTDE) was made with the purpose of providing access to the surface of a natural water-conducting fracture for in situ diffusion and sorption experiments at ambient chemical and rock stress conditions. The geometry of the experimental borehole was governed by identification of a suitable target fracture at about 10 m depth in the nearby collared pilot borehole KA3065A02. Fracture identification in the pilot boreholes was made using borehole imaging (BIPS) and difference flow logging. The telescoped borehole was drilled with a diameter of 300 mm up till about 1 metre away from the target structure. Drilling at 196.5 mm diameter continued up till the target fracture and lightly beyond. The outcome was a 160 mm stub, some 3 times longer than originally planned. BIPS imaging and core logging in the two boreholes were used to correlate fractures in the two holes. The correlation was substantiated by mineralogy and geochemical studies including stable isotopes. The fact that the borehole stub turned out three times longer than expected questioned the possibility to study in situ diffusion in intact rock. Analysis of the site specific conditions using both micro seismics, thin section analyses and numerical modelling, showed that the core stub was significantly damaged. As a resolve the experimental concept, previously focused on sorption phenomena at the target fracture surface and axial diffusion in the core stub into the intact rock, was changed. By accessing a portion of intact rock by extending the experimental borehole with a 36 mm section, the sorption component can be retained as planned and in situ radial diffusion in the intact rock can be studied. The fracture information from beyond the target fracture in KA3065A02 was used to optimise the slim hole drilling. An extension of about one meter was drilled. Using information from the two boreholes the three-dimensional structural and geological model of the experimental volume was subsequently updated to serve as a basis for completing the experimental borehole with a suitable packer system.

Sammanfattning

Borrning av ett experimentborrhål för LTDE genomfördes för att ge åtkomst till en naturligt vattenförande spricka för diffusions- och sorptionsförsök under naturliga kemiska och bergmekaniska förhållanden. Geometrin på experimentborrhålet bestämdes på basis av identifierad lämplig spricka på c:a 10 m djup i det närbelägna pilotborrhålet KA3065A02. Kartering av sprickor i de två borrhålen gjordes med hjälp av borrhåls-TV (BIPS), kärnkartering samt differensflödesloggning. Det teleskoputformade experimentborrhålet borrades med diameter 300 mm (277 mm kärna) ner till c:a en meter från målstrukturen varefter en diameter av 196,5 (177 mm kärna) utnyttjades fram till målstrukturen och något därbortom. Resultatet blev en 160 mm lång kvarvarande ”kärnstubbe” i borrhålet, c:a 3 gånger så lång som tidigare planerat. BIPS-data och kärnkarteringsdata från de två borrhålen utnyttjades för att korrelera sprickor mellan borrhålen. Denna koppling understöddes av mineralogi och geokemiska analyser av sprickmineral, inklusive analys av stabila kol- och syreisotoper. Eftersom kärnstubben blev tre gånger längre än planerat ifrågasattes möjligheten att utnyttja det ursprungliga experimentupplägget för att studera diffusion i intakt berg. Analys av de platspecifika förhållandena med hjälp av mikroseismik, tunnslip och numerisk modellering, har påvisat en trolig hög grad av skada på den kvarvarande kärnstubben. Som ett resultat ändrades det experimentella konceptet, som ursprungligen fokuserades på sorption på sprickytan och axiell diffusion genom kärnstubben in i det intakta berget därbortom. Genom att nå det intakta berget med en förlängning av borrhålet med 36 mm diameter, kan sorptionskomponenten behållas som planerat och radiell diffusion från förlängningen in i det intakta berget studeras. Sprickinformation bortom målstrukturen i KA3065A02 utnyttjades för att optimera förlängningen av KA3065A03. Borrhålet förlängdes med c:a 1 meter. Information från förlängningen utnyttjades för att uppdatera den tre-dimensionella strukturgeologiska modellen av experimentvolymen. Denna låg sedan till grund för design av manschettsystemet i experimentborrhålet.

Foreword

The results and analysis presented in this report would not be possible without the active participation and interaction with a number of individuals. Among these are;

Göran Nilsson, GNC AB

Christer Gustafsson, Malå Geoscioences AB

Lars Andersson, SKB (On-site coordinator)

Jarmo Mäkkinen, Drillcon AB

Christer Eriksson, Geocon AB

Chun-Lin Li, Boliden Mineral AB

Matti Hakala, Gridpoint Oy

Pekka Rouhiainen, PRG-Tec Oy

Jari Pöllänen, PRG-Tec Oy

Berngt Gentzschein, GEOSIGMA AB

Contents

1 Introduction

The objective of the Long-Term Diffusion Experiment (LTDE), Byegård et al. (1999) was originally to study the magnitude and extent of matrix diffusion from a natural fracture surface, through the altered zone, into the intact matrix rock. Further, to compare obtained *in situ* values on diffusivity with that obtained from corresponding studies on core samples in the laboratory. The experimental concept involves drilling of a telescoped large-diameter borehole to intercept a target feature identified in an existing small diameter pilot borehole some 10 m away from the Äspö access tunnel. The feature is packed-off using a special packer which seals around the developed core stub. The borehole is further packed of with mechanical and inflatable packers to avoid effects of the acting hydraulic gradient towards the tunnel. A tracer solution consisting of conservative and sorbing radioactive tracers will be circulated in the section with the natural fracture for a period of 3-4 years. A penetration due to diffusion in the order of decimetres was expected over the duration of the experiment. Subsequently, the rock volume subject to diffusion will be over-cored, sectioned and analysed for tracer activity/concentration. The *in situ* experimentation is supported by various types of mineralogical, geochemical and petrophysical analyses.

The proposed location for the LTDE is located in the niche at tunnel section 3/065 m at a depth of approximately -400 masl. Borehole KA3065A02 served as exploration pilot borehole to find a suitable target structure on which to perform the experiment. The target structure is required to fulfil a number of technical criteria which are related to experimental equipment, geometry and geology of the rock mass. The main requirements of the geometry and geology of a potential experimental candidate are summarised below:

- Oriented as close to orthogonal to the borehole axis as possible for optimal fitting of the customised packer, or “cup”, which will isolate the exposed fracture surface and the 50 mm long core stub,
- No fracturing beyond the target within a distance in the order of approximately 15 cm to ensure a stable core stub and diffusion in intact matrix rock,
- Single fracture plane to ensure a planar fracture face,
- Hydraulically conductive structure desired (representative conductive structure)
- Fracture mineralization and/or an altered rim zone,
- Located at a convenient depth (< 20 m away from the tunnel system) for practical reasons, but satisfactory far off (> 5 m) from the tunnel system to be unaffected by excavation damage and stress relief,
- Representative fracture for the rock mass at “deposition hole scale” in the Äspö HRL, i.e. devoid of coatings with unusual minerals or alteration mineralization,

The experimental borehole was drilled early 2000 and the outcome was that a 3 times longer core stub than expected was obtained. This initiated analysis to assess the effects of this fact on the experiment. These studies included laboratory tests and rock mechanical modelling to assess the damage and inherent effects on assessing *in situ* diffusivity. The outcome was that an experiment focused entirely on the core stub would be futile, resulting in data applicable only to stress-unloaded rock. Instead, early ideas to develop a test section in intact rock were revisited. The resulting modified test scheme included drilling of a slim-hole extension, 36 mm in diameter, through the 150 mm core stub and into intact rock. In the slim-hole extension a test section could be devised whereby radial diffusion from the borehole could be achieved. By employing a sequential approach (axial) diffusion/sorption in conjunction with the target structure surface and the (stress unloaded) core stub can be combined with (radial) diffusion in intact rock under ambient stress conditions. The possibility to find such portions of intact rock was analysed using data from KA3065A02 and conditions were found favourable. Drilling of the slim-hole extension was realised in October 2001.

The present report summarises the drilling, site characterisation, laboratory and modelling efforts made during 2000-2002 to provide a functional experimental site for LTDE. Chapters 2 and 3 review the results of drilling and characterisation of boreholes KA3065A02 and KA3065A03. Chapter 4 is devoted to attempts to correlate fractures between the two boreholes using physical attributes and mineralogy/geochemistry. Furthermore, the characteristic of the experimental volume which hosts the target structure and the intact rock section is discussed including a full 3D descriptive structural model. The concluding Chapter 5 accounts for the analysis of sample disturbance which predated the development of an alternative experimental concept. Chapter 6 provides discussion and conclusions drawn.

In the following, if not explicitly expressed otherwise, the borehole coordinates in KA3065A02 and KA3065A03 in the text, graphs and tables are related to the collar of the metal casing sticking out of the boreholes. In the case of KA3065A03 the stickup of the casing is 0.478 m from the rock surface.

2 Overview of characterisation in KA3065A02

2.1 Potential experimental candidates

Borehole KA3065A02 has been investigated by BIPS logging, POSIVA flow logging and radar measurements. The results of these investigations are reviewed by Winberg et al. (2000). Potential water-bearing fractures have been identified by correlating significant flow anomalies in the POSIVA log to identified geological features along the borehole. The geological characteristics for fractures associated with POSIVA flow anomalies are summarised in Table 2-1. The POSIVA flow log is presented in Figure 2-1.

Table 2-1 Potential experimental candidate structures in borehole KA3065A02.

6.54 m		Not a candidate due to its zone-like character and the close proximity to the tunnel.
7.96 m	331/8	Chlorite filling in a fracture with a close to orthogonal orientation to the borehole axis. The fracture surface is worn down due to rotation of the core during drilling.
9.34 m 9.37 m 9.40 m 9.43 m 9.45 m	350/89 151/77 155/80 162/65 164/81	Inflow of 16.1 l/min in a complex zone of at least 5 fractures distributed over a distance of 15 cm. Not suitable.
9.81 m	140/81 (main fault) (cf. Figure 2-1)	Main fault with slicken lines on fault surface. Mylonitic character in greenstone/diorite with increasing alteration towards the fault centre. 5 fractures over a length of 25 cm, where at least the two bottom most fractures are not included in the BOREMAP mapping. The associated BIPS picture is bad due to a large inflow of water and degassing. Suitable candidate located beyond main fault as good rock is penetrated just beyond these features.
11.9 m	116/33	Sealed, not suitable
12.6 m	115/90	Calcite-chlorite filled fracture in diorite with no or very little rim zone. Possible target as good rock is penetrated below the feature (approx 30 cm). Homogeneous rock with few fractures. The angle to the borehole axis is relatively small making this feature a somewhat more difficult target. There is a fracture just below this one with an orientation of 154/51. The two fractures will intersect if they are extended outwards from the borehole making this a less suitable candidate.
18.98 – 19.04 m	325/70	A section of four calcite-chlorite filled fractures over a distance of approximately 10 cm in homogeneous greenstone. 40 cm below this section there is homogeneous greenstone with a few sealed calcite-chlorite-epidote filled thin fractures.
23.2 m	155/68	Chlorite-calcite filled fracture in a complex fractured section with cross-cutting open structures and a mixed rock of greenstone and fine-grained granite. Not suitable due to cross-cutting features.

23.6-23.7m		Complex fracturing in a section of fine-grained granite. Chlorite filling. Not suitable due to the complexity of the fracturing.
23.79 m (23.86)	153/82 (233/52)	Calcite filled fracture in a thick section of greenstone. Above the fracture there is a large package of other faults and fractures. Beyond, the core is homogeneous and no fractures over a distance of approximately 1 m are found. Just above the target, there is one unmapped fracture with an orientation parallel to the borehole axis. This feature is a possible candidate due to its geometry. However, there are several issues that make this less structure attractive; the fracture is possibly associated with a crosscutting feature, the fracture occur in greenstone and the larger package of faults may interfere with the fracture away from the borehole.
42.8 m	332/76	This calcite-chorite filled fracture cuts both aplite and diorite and is almost orthogonal to the borehole axis. There is another calcite fracture cross-cutting the target. Not suitable due to both cross-cutting and dual rock types.
43.87	141/84	Calcite-chlorite-epidote filled fracture with cross-cutting (though sealed) fractures almost parallel to the drill core. The fracture surface is worn due to rotation of the core during drilling.
45.24 m	337/89	Fracture with a rim zone located in diorite. The fracture filling is both chlorite and calcite. A fracture almost parallel to this feature cross-cuts the target. Not suitable due to the cross-cutting of two fractures.

The selected target structures are the fractures associated with the main fault at 9.81 m in KA3065A02, c.f. Figure 2-2. The selection is made mainly on the basis of;

- Simple geometry
- Homogeneous geology
- Intact piece of rock beyond target structure (> 0.5 m)
- Hydraulics (inflow)

The fractures are minor, but cut the core below a fault and mark the beginning of a larger section (> 50 cm) of non-fractured diorite. The determination of the orientation is not well established due to the poor condition of the BIPS log. Large inflows and degassing occur at 9.4 m that makes the image blurred, and fracture orientations are difficult to estimate. An effort was made to roughly estimate the orientation of the features at L=9.90 and 9.84 m to 328/88 and 138/80, respectively.

Note : A repeated BIPS measurement was performed in the borehole with a new RAAX BIPS 4 equipment (doubled resolution). This measurement overall confirmed the geometry found in the original measurement with the equipment owned by SKB.

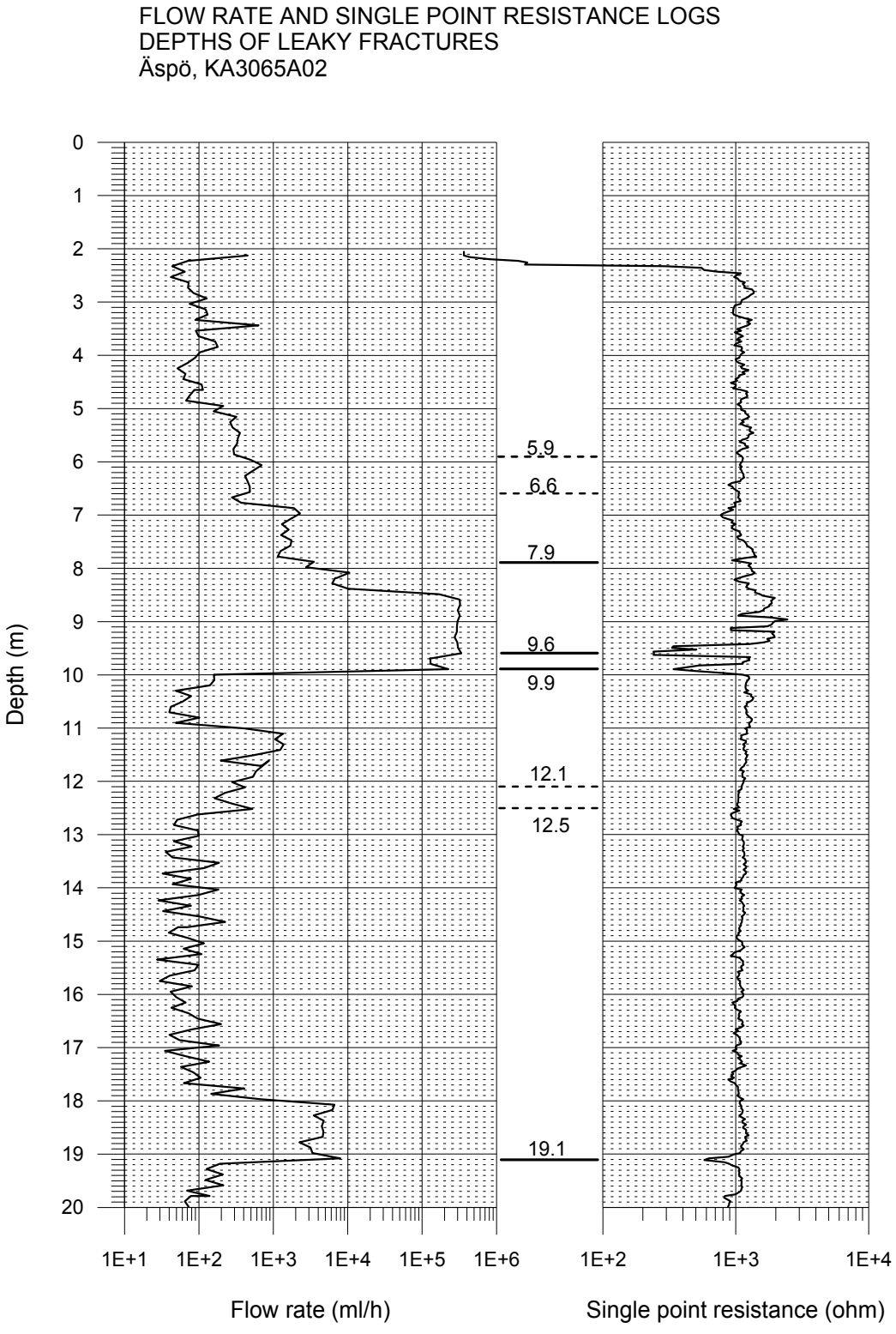

Figure 2-1. *Results of POSIVA flow logging in KA3065A02, L=0-20m*

Figure 2-2. *The main fault in KA3065A02 at L=9.81 m. The two fractures below the "main fault" (cf. slab in lower box at coordinate 80 cm) are interpreted to be splay fractures to the fault of which the lowermost is the proposed target fracture.*

2.2 Structural model based on pilot borehole KA3065A02

The structural model was focussed on conceptualising the detailed fracturing around KA3065A02 and the identified target feature at L=9.90 m. The objective was to propose an orientation and location of the experimental borehole such that the target feature would be intersected with as much confidence as possible. The experimental setup also requires that the target fracture is intersected as close to an orthogonal angle as possible. Further, the structural model aimed to provide the length coordinates of projected intersections in the planned experimental borehole of structures identified in the pilot borehole, located prior to the target fracture. To achieve this, fractures that were interpreted to be large enough to intersect a borehole at a maximum distance of 2 m were included in the model. Fractures that qualify are

- Identified conductive structures/fractures (from the POSIVA log)
- Fractures mapped as "natural" in the BOREMAP system

The general approach was that identified structures in KA3065A02 were extended in a planar fashion along their strike orientations. An artificial experimental borehole with a 300 mm diameter was then placed in the model such that the angle to the target fracture was close to orthogonal and the minimum distance between the mantel surfaces of the boreholes was 30 cm. The starting point of the borehole was located such that it was possible to locate the drill rig to a suitable collar position.

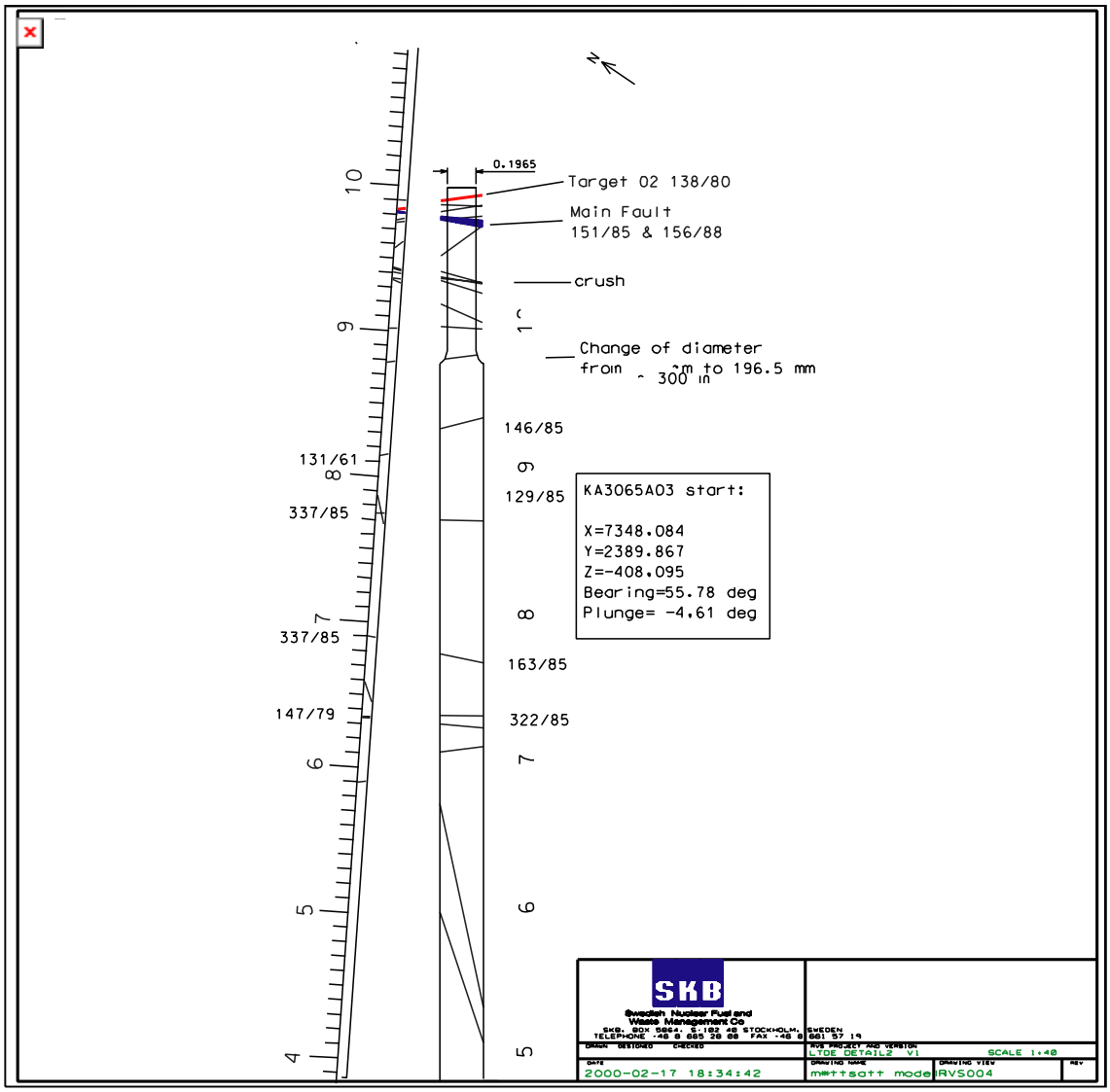

Figure 2-3. *Illustration of the structural model around KA3065A02. The visualisation of the proposed borehole KA3065A03 contains the location and orientation of the predicted orientations. The diameter changes from 300 mm to 196.5 mm, less than 1 m away from the target structure. Section illustrated along a plane through the centre of the proposed borehole KA3065A03.*

2.3 Experimental borehole KA3065A03

A trial and error approach was used to find the optimum orientation of the experimental borehole based on the geometrical constraints of near orthogonality of the target structure and a minimum distance of 30 cm between the borehole mantel surfaces. The diameter of the experimental borehole is 300 mm from the stub down to approximately less than a metre away from the target fracture. The diameter then changes to 196 mm down to the target fracture. The minimum distance between the boreholes was set to 30 cm, which means that the minimum distance between the axises of the 56 mm and 196 mm boreholes is 42.6 cm.

The optimum orientation was found by rotating the end of an artificial experimental borehole along a circle with radius 42.6 cm centred on KA3065A02 at L=9.90 m. The start of the artificial experimental borehole was then fixed to the best drilling position on the tunnel wall. The final orientation was set in the direction where the target structure was predicted to be the last intersected structure before entering into a section of unfractured Ävrö granite. The depth to the target fracture in the experimental borehole was estimated to approximately 10.35 m. The drilling depth was therefore targeted to be L=10.40 m to have an approximately 5 cm long stub to facilitate isolation of the exposed fracture surface using a tailored "cup-shaped" packer. Immediately before intercepting the identified target feature, a relatively large fault is intercepted with associated fractures. The target fracture is interpreted to be part of this system.

The surveyed collar coordinates for the experimental borehole orientation are given by Table 2-2.

Table 2-2. Collar coordinates (on the borehole wall) and borehole geometry for KA3065A03.

Northings:	7348.075 m
Eastings:	2389.873 m
Z :	-408.092 masl
Bearing:	55.77 °
Inclination:	-4.52° (down)

3 Overview of characterisation in KA3065A03

3.1 Introduction

The drilling of KA3065A03 employed a very intricate interactive approach involving many geoscientific disciplines. A site geologist was on site during the whole drilling process to handle the cores and to keep the drilling record. During the later phases of drilling (L> 8 m), the site geologist was seconded by a logging engineer (BIPS logging), a member of the HRL Experimental services team, who provided Pearpoint borehole video imaging. In addition, the responsible structural geologist was present, computer and RVS model in hand, to keep a continuous track of the outcome in relation to the predictions made, and to make the necessary revisions and updates of the model accordingly. All this with the objective to terminate the borehole at a pre-set desired depth, leaving a 50 mm core stub at the bottom of the borehole.

During the drilling, pressure registration was made in packed-off test sections established in KA3065A02 between 3-13 m and 14-70 m, respectively. Data was collected on a Borre portable logger.

Eventually, the borehole turned out to be somewhat too long, leaving a 150 mm stub in the borehole. Measures were subsequently taken to map the topography of the stub's end surface using ia. borehole video, manual and geodetic measurements. In addition, a 6 mm video endoscope was used to map the 9.75 mm slot between the stub and the borehole wall to ensure that no macro fractures exist in the 150 mm deep annular slot around the core stub.

In the attempt to reconcile the interpreted structural information in the pilot borehole (KA3065A02) with that of the outcome of the LTDE experimental borehole (KA3065A03) a very good match between the predictions and outcome is found in places in the first 9 metres, whereas in other places the match is poor, cf. Chapter 4. However, in the inner parts of the borehole a clear discrepancy was noted between the predictions and the outcome, particularly with regards to the geometry of the structures, cf. Section 3.2. In order to verify that the noted discrepancy was not due to the BIPS measurements, having been done at two separate occasions with two different systems, the BIPS measurements were repeated with the RAAX BIPS 4 equipment.

3.2 Drilling of KA3065A03

3.2.1 300/196.5 mm

Drilling of the experimental borehole KA3065A03 was performed using a Hagby Bruk Onram 1000 rig. The core drilling of the initial 300 mm portion of the experimental borehole started January 31, 2000 and was finished February 3. The 300 mm drilling stopped at a depth of 9.20 m. A conical transition zone was created with a special adapter, reducing the borehole diameter to 196.5 mm. The 196.5 mm drilling started at borehole depth 9.762 m and was continued down to 10.883 m, after which the equipment was retrieved with a 25 cm stub remaining in the hole. Very poor visibility in the hole was noted due to a very high inflow and degassing. After rinsing of the hole, followed by Pearpoint TV inspection, it was decided to proceed another 5 cm to

intercept the assumed cm wide chlorite-filled main fault seen at L = 9.81 m in KA3065A02, cf. Figure 2-1. The "target structure" was predicted at L=10.778-10.828 m. In this context it should be noted that the projection of the innermost structures in KA3065A02 suffer from uncertain orientations associated with poor BIPS imaging. The latter due to high water inflow and degassing into borehole KA3065A02 during the BIPS measurements.

The drill stem was subsequently mounted back in the hole and the drilling was recommenced, this time at a very slow pace. The core most likely broke during this operation. After drilling some additional 5 cm to L=10.728 m, the loose core segment was retrieved using the "core barrel ring". The depth of the break was calculated to L=10.718 m. The lowermost surface of the retrieved core exposed a fresh surface, orthogonal to the axis of the hole, and partly polished. At this time it was decided to continue drilling in 5 cm sections to a maximum depth of L=10.40 m, with a continuous careful monitoring of pressure changes in the pilot borehole and changes in inflow to the borehole. After each section the drill stem was partly retrieved (with core barrel ring in place) to check whether the stub had come loose. It was however impossible to break the stub and the drilling was continued, with no noted changes in inflow and pressure, down to a final depth of L=10.878 m, at which drilling operations were terminated on February 7.

When retrieving the drill stem, it was noted that parts of the drill core were found in the core barrel. These parts are interpreted to belong to the main fault. Repeated measurements verified that the surface of the stub is located at a depth of L=10.718 m, implying a remaining stub in the order of 160 mm, compared to the originally desired length of 50 mm. A plausible account for the line of events leading up to the outcome is the following; the lowermost parts of the core in the last uptake (at L=10.728 m) fell out of the core barrel and were submerged under water, such that a fresh break in the core was noted when inspecting the lower end of the core in the barrel. The core barrel collected the fragments when reentering the drill stem again. In addition, the structures noted beyond the master fault in the pilot borehole, notwithstanding the close proximity to the experimental borehole (40 cm), appear to converge towards the experimental borehole, or alternatively terminate between the two holes.

After a period of rinsing, vacuum pumping etc., the surface of the stub was identified as a fracture surface in part covered by chlorite and calcite. Additional parts of the main fault, which had remained on the bottom of the hole, were retrieved during the cleaning and rinsing operations.

3.2.2 36 mm

Following the outcome of the drilling and subsequent characterisation and analysis, a new experimental concept was formulated which included not only circulation of tracer solution across the surface of the target structure (promoting axial diffusion), but also circulation in an inner test section (promoting radial diffusion) in intact bedrock beyond the target structure. Following a geological assessment of the feasibility of finding a suitable section and feasibility of docking suitable equipment for a slim hole to the existing equipment, plans for drilling a 36 mm extension commenced. The main problem areas were associated with; 1) prediction of fracturing ahead of the core stub, 2) drilling of the slim hole without damaging the core stub and extracting slim core.

Based on information from KA3065A02, 1-2 fractures were deemed likely to occur immediately beyond the root of the 150 mm core stub, interpreted to be non-conductive. Portions of intact non-fractured rock were projected between 10.7 and 11.2 m (between fractures #10 and #13 and between fractures #12 and #14, cf. Chapter 4). Of the 5 interpreted and projected fractures assumed to occur in the planned extension of the 36 mm slim hole, fractures #12-#14 were assumed "naturally open" and #11 and #15 as "naturally sealed". Of the former, water flow was only assumed associated with Fracture #14.

The drilling was carried out successfully early October 2001 using an electrical ONRAM 1000 drill rig. A 76 mm drill stem was employed with a 36 mm adapter enabling collection of 22 mm cores. The double-tube core barrel of standard type was 1.5 m long enabling retrieval of core lengths shorter than 1.5 m.

As the knowledge concerning the structure beyond the stub was limited, a first section of 45 cm was drilled. Only one sealed fracture, located at L=11.137 m, was observed in the associated drill core. A section of almost 0.3 m intact, almost unaltered Ävrö granite was identified from L=10.8 to L=11.1 m. However, it was considered that the first and last 5 cms of this intact rock section might not be suitable because of the influence of the stub (upper portion) and the fracture (lower portion). Consequently, in order to see whether a longer more suitable intact section of rock could be identified further in to the rock, the borehole was extended another 60 cm. The total length of the 36 mm extension is 1.085 m. Two natural fractures were identified in the second uptake, at L=11.347 and L=11.637 m, respectively. The fracture at the very bottom of the extension (L=11.822 m) may also be natural. These fractures show small angles relative to the axis of the core.

Analysis of the outcome of the two 36 mm drilled sections identified a section in the upper core section, from L=10.8 to L=11.1 m, as the most suitable for the planned diffusion experiment in intact rock.

The rock mass beyond the stub root was found to be intact with some minor portions with altered (red-coloured) rock and, with a few exceptions, essentially devoid of natural fractures. A section, about 35-40 cm in length was identified as the prime candidate for the test section in the intact rock. Subsequent flow tests have identified one fracture (#14) in the interior of the slim hole to be conductive, and connected to the neighbouring pilot borehole KA3065A02, cf. Section 3.4.

3.3 Fractures in KA3065A03

3.3.1 Observed fracturing in KA3065A03

The observed fracturing in KA3065A03 down to a depth of 11.82 m is listed in Table 3-1. The observations in Table 3-1 are based on core observations and on the initial BIPS logging of the borehole shortly after the completion of drilling. The BIPS logging is not available below 10.429m depth. Observations are then only based on core mapping and video imaging. The actual fracture locations in the experimental borehole are illustrated in Figure 3-1.

Table 3-1. Location of fractures in KA3065A03. Fracture orientations are derived both from initial BIPS measurements and core inspection. Fractures denoted with (*) are only visible in the core and are oriented only by the angle relative to the borehole axis (alfa angle). In addition to the observed centre point of intersection for each fracture, minimum and maximum distances are calculated for the intersection with the circumference of the borehole.

Intersection depth (centre point in metres) - metal casing	Orientation strike/dip (alfa angle*)		Intersection with circumference (m)		Geology/Hydraulics
	Strike	Dip	Min	Max	
0.899*	70*				Ca
0.969*	70*				Ca
1.539*	5*		1.06	3.98	Sealed, Ca
1.979*	70*				Chl, Ca
2.189*	45*				Sealed, Ep 2-4 mm
2.359	142	74	1.84	1.92	Chl
6.809*	60*				Sealed, Ca
6.929*	75*				Sealed, Ca, 1 mm
7.199*	85*				Sealed, Ca, 1 mm
7.249	142	87	6.76	6.78	Ca
7.419*	65*				Chl, Ca
7.599*	50*				Sealed, Chl
7.659*	80*				Chl
7.709	163	83	7.18	7.28	Chl
8.329	147	66	7.80	7.90	Chl, Ca, 1 mm
8.729*	90*				Chl, crush
8.779	141	86	8.28	8.32	Chl, crush
8.859*	80*				Sealed, Chl
9.289*	40*				Sealed, Chl, Ca, 2 mm
9.489*	80*				Sealed, Ca
9.659	?	?			Sealed, Ep
9.679	163	86	9.15	9.25	Chl / 0.5 l/min
9.939	129	72	9.42	9.50	Chlorite / drops
10.059	324	88	9.57	9.59	chlorite
10.079	147	71	9.58	9.62	Chl, Ca, 12 l/min[(1)]
10.149	132	84	9.64	9.70	Chl, Ca 12l/min[(1)]
10.169	118	60	9.62	9.76	Chl, 12 l/min[(1)]
10.369	168	83	9.86	9.92	Chl
10.429	168	75	9.91	9.99	Chl
10.429	157	68	9.92	9.98	Chl
10.737*	134	85.4			Sealed
11.137*	8.4	82.7			Sealed
11.167*	132	85.4			Natural?
11.327*	315.9	84.6			Sealed, Chlorite
11.347*	310	79.6			Ca, Chlorite
11.387*	2.1	63			Sealed
11.427*	6.3	67.8			Sealed
11.637*	338.4	54.2			Chlorite, Ca
11.822*	125.9	85.4			Natural?

[1] *The inflow is 12 l/min for the whole borehole section*

The 300 mm section cuts through good quality Ävrö granite intersected by occasional fractures as shown in Figure 3-1. The Ävrö granite gradually changes in colour to more reddish with depth. There is practically no inflow before the transition zone from 300 mm to 196.5 mm. The fracturing increases after L=9.30 m. The first visible inflow point occurs in the transition zone, in the fracture at L=9.679 m (Table 3-1). The Ävrö granite is altered between L=9.9 m to L=10.38 m, which is also indicated by core crush between L=10.08 and L=10.28 m. Water inflow of around 12 l/min is observed in this section through several inflow points. Below there is a section of non-fractured greyish Ävrö granite between L=10.38 to L=10.71 m. Then, the fracture surface forming the face of the stub (L=10.719 m) is a splay fracture to the main fault, which is located immediately before the face of the stub. The Ävrö granite turns reddish closer to the main fault. This splay fracture is not the predicted target structure, which was interpreted to intersect at approximately L=10.83 m, further down in the remaining part of the stub.

Thin sealed fractures intersect the 36-mm section between L=10.73 and L=10.75 m, which means inside the remaining stub of the 196.5-mm section. These are identified as splay fractures to the main fault. The tectonic reddish Ävrö granite is identified down to around L=10.76 m. These seem to be directly related to the main fault and the associated fractures surrounding the main fault plane. However, the identification of one of these fractures as the predicted target structure is not obvious. From L=10.76 to around L=10.85 m, the rock is a reddish Ävrö granite. The 196.5-mm section stops at L=10.88 m. From L=10.85 m down to 11.822 m (end of the 36-mm section), the borehole is intersected by more occasional fractures, see Table 3-1. The rock is a greyish Ävrö granite, except for two reddish sections, from L=11.077 to L=11.167 m, and from L=11.347 to L=11.477 m. Water inflow of 2.6 E-05 l/min is observed in the 36 mm-section. The conductive fracture is most probably at L=11.637 m. There may exist hydraulic connectivity between the conductive fractures in KA3065A02 and KA3065A03.

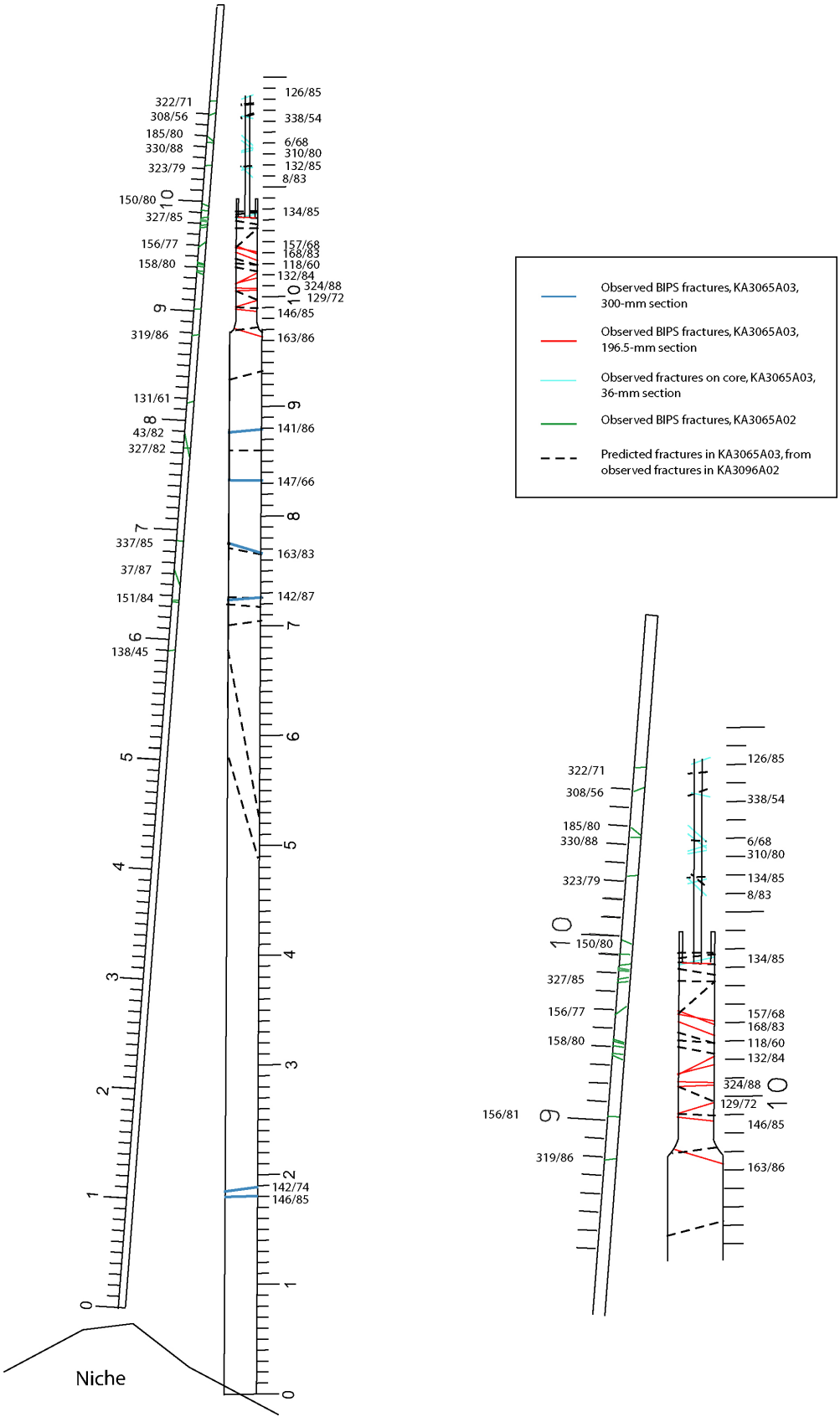

Figure 3-1 *Illustration of the location of the observed fractures in KA3065A02 and KA3065A03 (including 36 mm section) as mapped and logged from the initial BIPS measurements and core observations. Hatched black traces in KA3065A03 show the predicted locations based on KA3065A02 data.*

3.3.2 Correlation of observed and predicted structures

The fracturing in the 300 mm section of the experimental borehole KA3065A03 shows a good match with the intersections predicted from fracture data in KA3065A02. However, the actual fracture orientations in the inner parts (196.5 and 36 mm sections) of the borehole deviate from the predicted orientations.

Extensive investigations and analysis to find possible reasons for the latter mismatch have been performed in the 196.5 mm section. A new high resolution BIPS logging (BIPS 4) has been performed in both KA3065A02 and KA3065A03. The new data have been used to completely remodel the LTDE site in the Rock Visualisation System (RVS). The new data from KA3065A02 have been used to make new predictions to the locations and orientations in KA3065A03. Table 3-2 and Figure 3-2 show a compilation of the data sources in KA3065A02. The variation in the data between the different data sets is not considered large and generally fits well with the original measurements. Table 3-3 shows the two data sets available from the experimental borehole KA3065A03; 1) the original BIPS logging which was performed shortly after the drilling of the borehole and 2) the BIPS 4 logging using a new high resolution system with an improved light to produce better imaging of the borehole walls. The new data was compared to the original measurements and although there are a number of new structures found with the BIPS 4 tool, the fractures observed do not differ very much from the original measurements with the SKB BIPS tool. The deviation column in Table 3-3 shows the difference in strike and dip in the new investigation compared to the original BIPS data set. Most fractures are more or less aligned with fractures interpreted on the basis of the first set of measurements.

It is worth pointing out that the proposed target fracture projected from KA3065A02, which is interpreted as a splay to the main fault, is not observed in KA3065A03. This is quite remarkable, as the distance between the two boreholes at the depth in question, is less than 0.5 m.

Table 3-2. Data sources for fracture occurrences mapped in borehole KA3065A02.

BIPS interpretations in KA3065A02														
Original BIPS and core logging data			Correlation of inflow and BIPS based on the POSIVA flo						BIPS 4 data					
BIPS	strike	dip	Indikations in the POSIVA flow log (m)	ml/h	BIPS Bh length	strike	dip	comment	Bh length	strike	dip	Fractures not possible to correlate		
4.06	151	66	**5.9**	**5.00E+02**	**5.90**	**138**	**45**							
4.55	258	51	**6.6**	**4.00E+03**	6.50	37	87							
5.9	138	45			**6.35**	**147**	**79**							
6.31	146	81			**6.34**	**151**	**84**		6.38	150	85	4.32	184	80
6.34	151	84	**7**	**2.00E+03**	**6.90**	**337**	**85**		6.96	336	86	6.91	168	89
6.36	147	79	**7.9**	**3.00E+03**	**7.75**	**327**	**82**		7.80	329	77	7.91	149	73
6.54	37	87			7.75	43	82					7.99	159	82
6.88	333	88	**8.2**	**7.00E+03**	**8.15**	**131**	**61**	only a resistivity anomaly, the inflow occur just above this intercept	8.18	160	88	9.14	143	79
6.93	337	85	**8.9**	**(3.00E+05)**	**8.79**	**319**	**86**	inflow comes from 9.6 m?	8.82	318	82	9.54	156	77
7.75	327	82	**9.1**	**(3.00E+05)**	**9.02**	**149**	**77**	inflow comes from 9.6 m?	9.06	156	81			
7.96	331	78	**9.5**	**(3.00E+05)**	**9.43**	**164**	**81**	inflow comes from 9.6 m?						
8.17	131	61			9.34	350	89		9.42	350	88			
8.71	155	76			9.36	151	77		9.43	125	65			
8.78	319	86			9.40	155	80		9.69	294	39			
8.91	325	90			9.42	162	65							
9.03	149	77	**9.6**	**3.00E+05**	**9.60**	**293**	**42**							
9.37	163	86	**9.9**	**2.00E+05**	**9.90**	**328**	**88**	main target	9.84	136	73			
9.43	158	80			9.75	141	88							
9.44	151	85			9.77	137	83		9.89	156	88			
9.45	148	84			9.81	151	85	main fault	9.88	152	82			
9.51	163	73			9.82	156	88	main fault	9.9	147	83			
9.77	327	85			9.84	138	80		9.96	176	76			
9.81	140	81												
9.84	150	80	Data used in the prediction model											
9.85	156	84	Bold text indicate main structure if there are several possible in a short section											
10.33	323	79												
			An additional corelogging (red) was performed to try to define fracture orientations											
			in sections poorly covered by the initial BIPS analysis											

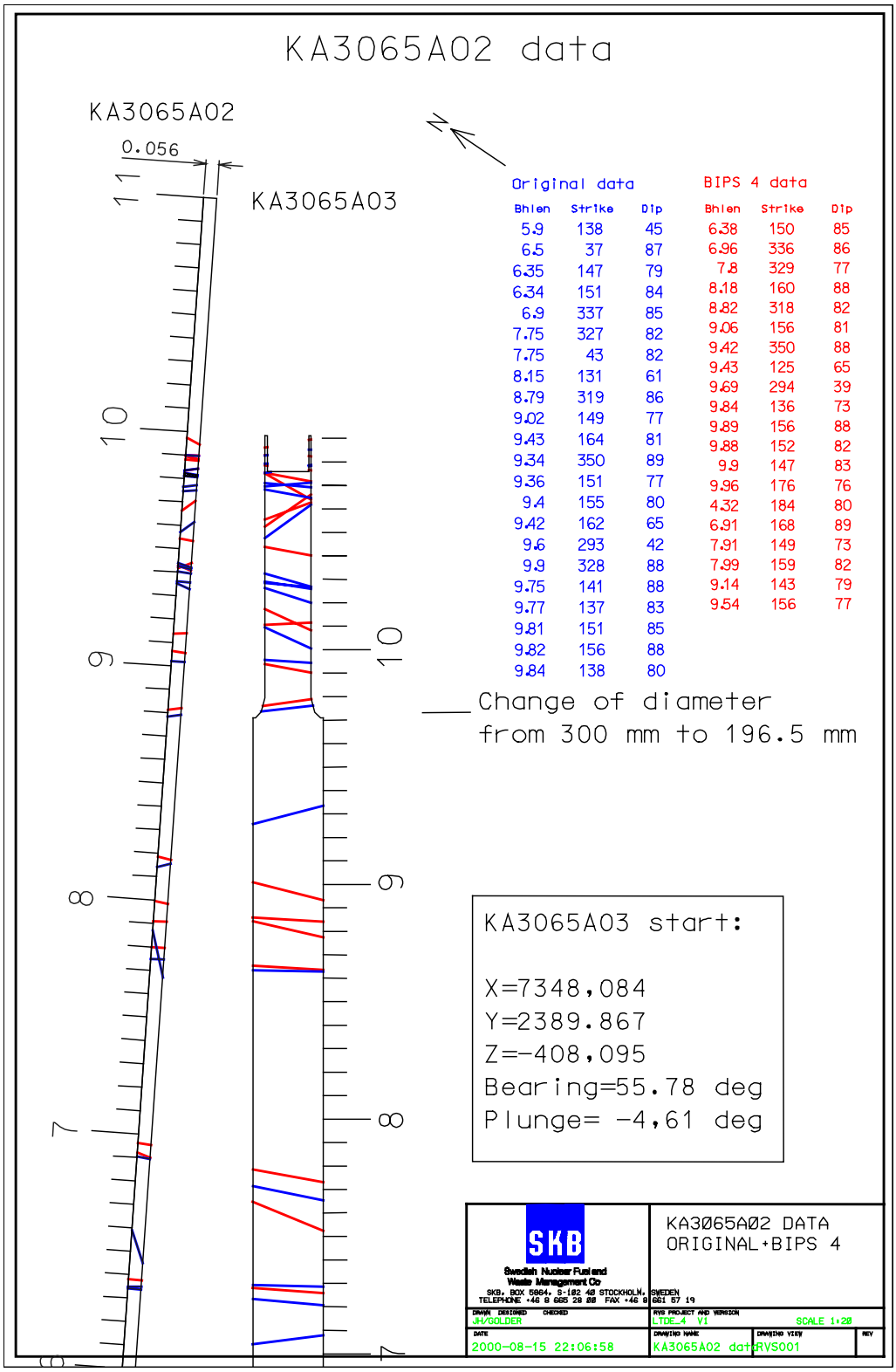

Figure 3-2. *Illustration of data sources for fracture occurrences in KA3065A02. The illustration shows the match between the original BIPS data with the BIPS 4 logging. Note that the new logging in KA3065A02 sampled a number of fractures not previously mapped as fractures. However, the initial measurements are a combination of core and BIPS analysis whereas the BIPS 4 analysis have been performed only by analysing the image, which limits the knowledge as to what is a fracture in comparison to combined BIPS/core observations.*

Table 3-3 Data sources for fracture occurrences in borehole KA3065A03.

BIPS interpretations in KA3065A03									
Initial BIPS interpretation in conjunction with the drilling				BIPS 4 interpretations 00-07-11					
							Deviation (Strike/dip) in cm	Fractures not previosly interpreted	
Bh length	Strike	Dip		Bh length	Strike	Dip			
2.30	146.00	85.00							
2.36	142.00	74.00							
7.25	142.00	87.00						10.013	143	75
7.71	163.00	83.00						10.1	158	7
8.33	147.00	66.00						10.21	326	85
8.78	141.00	86.00						10.479	145	87
9.68	163.00	86.00		9.683	165	85	2/1			
9.89	146.00	85.00		9.899	131	67	15/18			
9.94	129.00	72.00								
10.06	324.00	88.00								
10.08	147.00	71.00								
10.15	132.00	84.00								
10.17	118.00	60.00		10.161	120	60	2/0			
10.24	125.00	88.00								
10.37	168.00	83.00		10.365	170	83	2/0			
10.25	168.00	75.00		10.411	171	73	3/2			
10.25	157.00	68.00		10.421	156	64	1/4			
Mapped 2000-03-22										
					Almost perfect match					
					Pretty good					
					Is this the same fracture?					

3.3.3 Geometrical and structural-geological modelling

The new data was used to remodel the LTDE site using the RVS system. During the model development special attention was exercised to use the latest available SICADA data for borehole and tunnel locations. The model was built in 3D where each fracture in the borehole was generated at its mapped location as a disc. A section along each borehole was constructed showing the intersection point with each fracture as well as the line of orientation. Although the sections of the model are 2D planes along the boreholes, the map shown in Figures 3-1 and 3-3 are truly 3D as the borehole orientations are not identical. Individual chainage marks are therefore inserted for each borehole.

The final model showing the new BIPS 4 interpretations from both boreholes is shown in Figure 3-3. The difference between this model and the original model is shown in Figure 3-1 and lies mainly in the fact that the new BIPS logging revealed a few more fractures. The location and orientation of the fractures are still very similar. There is still a deviation between the predicted intercepts and the actually mapped fractures in the inner section of the experimental borehole.

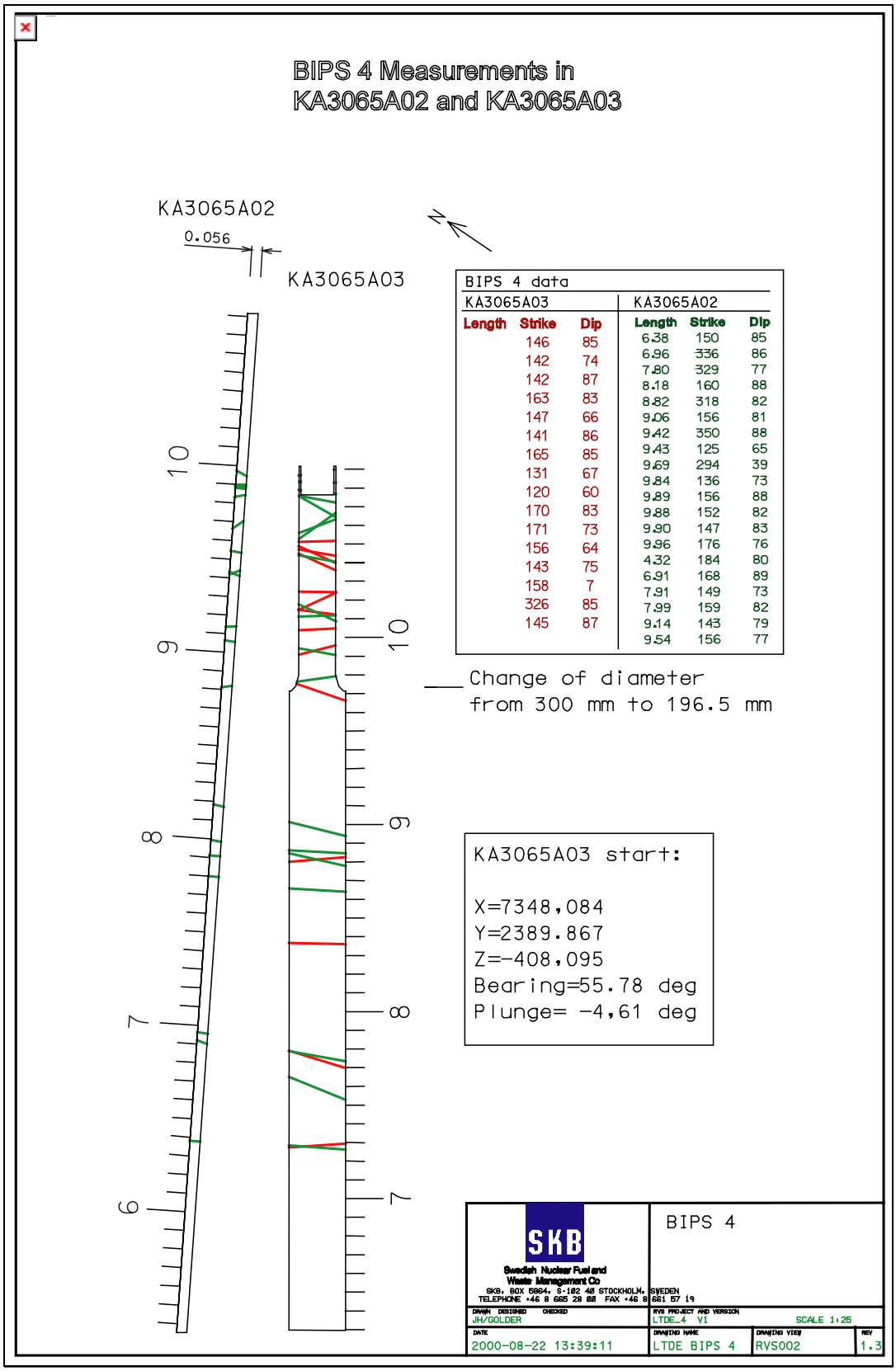

Figure 3-3 *Predicted intersections in KA3065A03 (green) based on BIPS 4 logging of KA3065A02 and the outcome after BIPS 4 measurements in KA3065A03 (red). The measurement in KA3065A03 is limited to a depth of 10.58 m due to hardware limitations of the BIPS equipmen .*

A 3D model is shown in Figure 3-4 with fractures generated in RVS together with the BIPS 4 image from L=9.68 to L=10.58 m in KA3065A03 and from L=8.7 to L=10.1 m in KA3065A02. The interpreted fractures are represented as discs and follow the mapped traces on the BIPS images more or less exactly. The model enhances the poor match in fracture orientation between both boreholes in the 196.5-mm section.

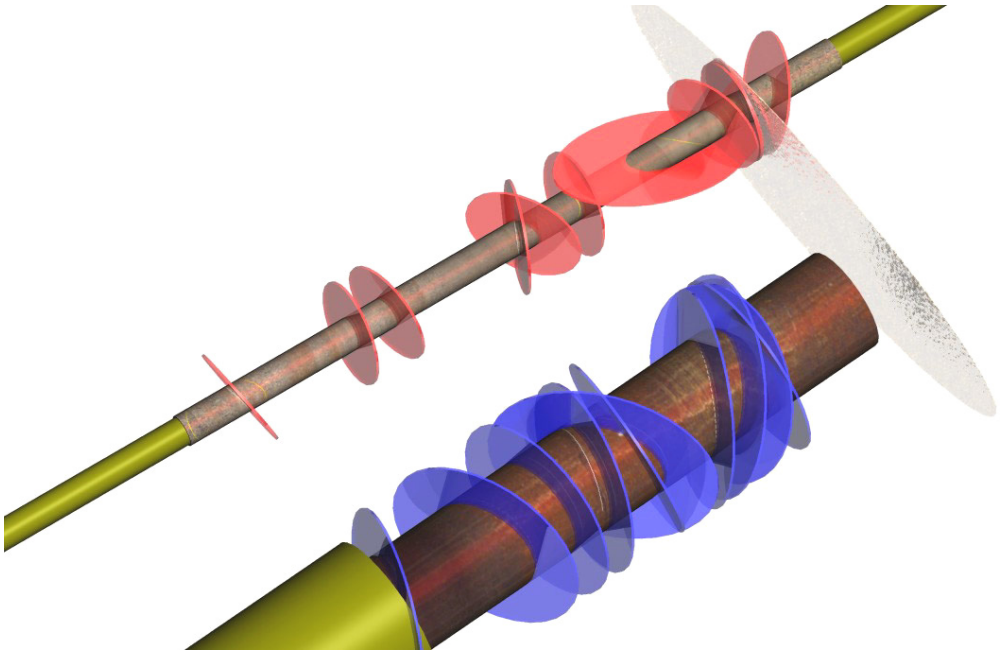

Figure 3-4. *A 3D view of fractures in the 196.5-mm section of KA3065A03 (blue discs) and in KA3065A02 (red discs). The model shows the BIPS 4 images (wrapped around the boreholes outlines) together with the RVS-generated fractures (discs). The match between the BIPS data and RVS discs is evident in this illustration, although some fractures are not visible due to the fact that they have no thickness. The grey fracture represents the target structure. North is up in the picture, cf. Figure 3-6.*

The actual fracturing in the 36-mm extension shows a quite poor correlation with the projected intersections (hatched) from fractures in KA3065A02, see Figure 3-5. Eight fractures were observed on the 36-mm core while five had been predicted from the BIPS measurements in KA3065A02.

BIPS interpretations in KA3065A03					
Initial predictions from BIPS 4 interpretation in KA3065A02			Mapped fractures in conjunction with drilling of the 36-mm hole		
Bh length	Strike	Dip	Bh length	Strike	Dip
			10.737	134	85.4
			11.137	8.4	82.7
11.199	323	79	11.167	132	85.4
11.389	330	88	11.327	315.9	84.6
11.209	185	80	11.347	310	79.6
11.659	323	79	11.387	2.1	63
11.759	322	71	11.427	6.3	67.8
			11.637	338.4	54.2
			11.822	125.9	85.4

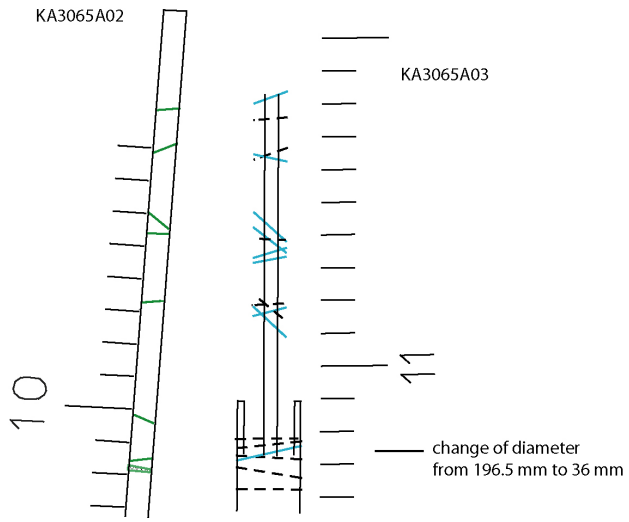

Figure 3-5 *Predicted intersections in KA3065A03 (black hatched traces) based on the BIPS 4 logging of KA3065A02 (green), and the outcome of core mapping in the 36-mm hole (light blue).*

Fracture data in the 36-mm section are from the core mapping. Fracture orientation was calculated from measured α and β angles on the core. These angles can be compared to the strike and dip of the fracture plane in the core relative to the coordinate system. If not defined when looking at the core the orientation of the relative coordinate system is obtained by using a clay plug to print the remaining stub in the hole. The strike and dip of fractures in the absolute coordinate system are then back-calculated by means of a rotation of the data in order to match the relative coordinate system to the absolute coordinate system. Endocope video imaging in the deep 36-mm section did not provide useful information on the fractures.

Mapping of fracture orientation from drill cores by means of alpha and beta angles may be a cause for discrepancy of strike and dip between predicted and actual fracture data. The values have not been calibrated to BIPS measurements. The hole is only 36 mm in diameter which may also affect the quality of the data. The smaller the diameter of the borehole, the greater the potential error in the determined alpha and beta angles might be.

The fractures that are observed in KA3065A03 but were not predicted from measurements in KA3065A02 are thin sealed fractures. Nevertheless, the distance between the two boreholes at this depth is less than 0.5 m.

Figure 3-6 is a 3D model of the 36-mm section in KA3065A03, from L=10.737 m to L=11.822 m and of the corresponding depth-section in KA3065A02. The discs represent actual fractures observed by BIPS measurements in KA3065A02 and core observations in KA3065A03.

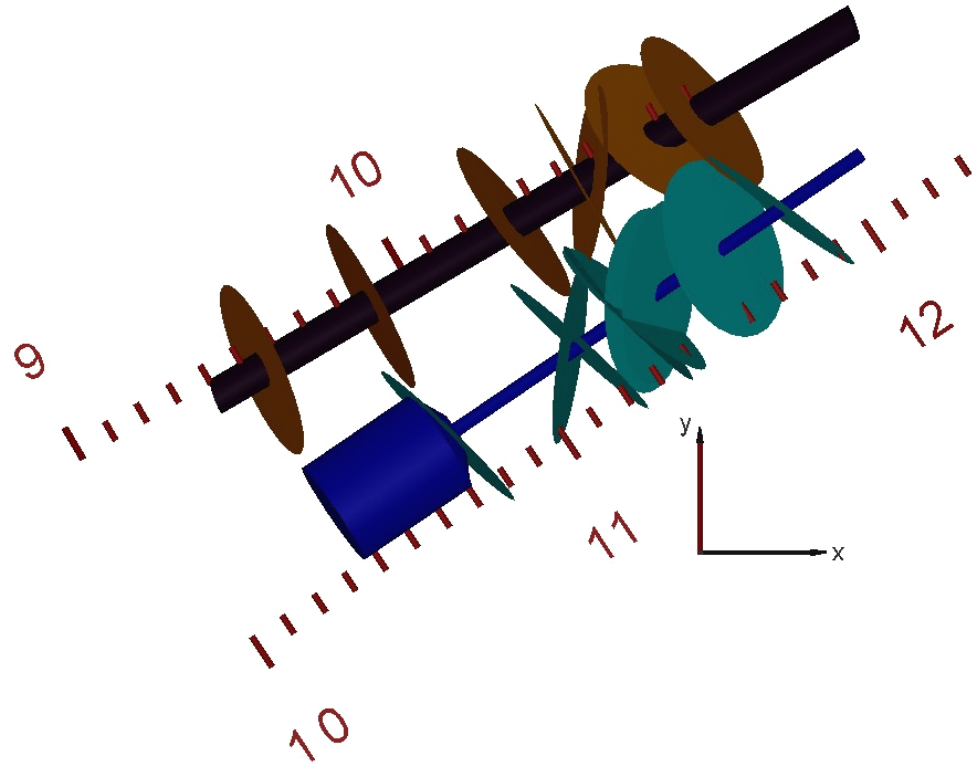

Figure 3-6. *3D view of the innermost sections of KA3065A02 (brown discs) and KA3065A03 (green discs). (y= North; x= East).*

The extensive model analysis does not reveal any major inconsistencies to the input data or to the construction of the model. The reasons for the apparent mismatch in orientation in the innermost sections of KA3065A03 must be found elsewhere. Two possible suggestions to the mismatch are;

1) there exists a discontinuity between the two boreholes that off-sets fractures in such a way that orientations are changed

2) orientations of the small fractures considered here vary greatly over short distances

The first hypothesis imposes other questions like; where is this fault? What impact does this have on the experiment? The second hypothesis suggests that fractures are so variable in extent and orientation such that it is difficult to trace any discontinuity over a longer distance than half a metre. However, previous experience at the Äspö HRL has shown that it is possible to interpret (extend) fractures in a more or less planar fashion over distances of several meters; TRUE-1 (Winberg et al., 2000) and TRUE Block Scale (Andersson et al., 2002). But it should be kept in mind that the latter fractures are of larger dignity, more comparable to the master fault of the target structure identified in both KA3065A02 and KA3065A03. It is still possible that smaller fractures, (e.g. splay fractures) are more difficult to predict. Furthermore, their radius may be just a few decimetres. The small diameter (36 mm) of the inner part of the KA3065A03 borehole also makes the determinations of orientation less precise.

3.4 Flow logging following drilling of 36 mm extension

Late October 2001 a series of single packer flow tests were conducted in the inner 36 mm extension of KA30565A02. The objective being to assess measurable flow in this part of the borehole and to identify possible hydraulic connection with the instrumented section P3 (7.5 m – 13.0 m) in KA3065A02. Using a specially devised single packer, three different sections of variable length were isolated in the 36 mm extension. The three sections yielded about the same flow at the collar (2.6×10^{-5} l/ min), indicating that the conductive fracture was located beyond the innermost packer position. A likely candidate is the fracture a t 11.637 m (#14, cf. Section 4.3). When section P3 in KA3065A02 was opened to atmospheric pressure, the flow at the collar of KA3065A03 was reduced by 20%, indicating hydraulic contact between KA3065A03:P3 and the innermost parts of the 36 mm extension.

4 Integrated model of experimental volume

4.1 Introduction

The following sections provides a detailed description of the target structure, as identified in borehole KA3065A02 and as identified in the experimental borehole KA3065A03 (Sections 4.2 through 4.5). In addition, the fractures and structures and the matrix rock beyond the target structure are described, including correlation of information (mineralogy and physical characteristics) between the two boreholes (Sections 4.2 through 4.4 and 4.6). A fully 3D model of the experimental volume including the target structure is presented in Section 4.4. The morphology of the surface of the target structure as seen in borehole KA3065A03 is presented in Section 4.5.

4.2 Correlation of fractures between boreholes

Fractures in the cores of KA3065A03 and KA3065A02 were correlated on the basis of orientation and macroscopic mineralogy as well as on observed flow, see Table 4-1. In order to assess the reliability in the correlation, three relative confidence measures were defined: low, good and high, which reflect both the quantity and quality of data used for the correlation.

The confidence measure for correlating fractures in the 196.5 mm section is considered good down to L=10 m in both boreholes. Orientation of fractures is determined by the BIPS measurements, whereas the mineralogical description is based on core mapping. For the section including the target structure, from L=10 to L=10.8m, the confidence measure can be considered as high. The orientation of fractures was checked against BIPS measurements, and the mineralogical description is based on core mapping complemented by detailed geochemical analyses of samples from both drill cores.

The measure of confidence for correlation of fractures in the 36 mm hole is considered low as no complementary geochemical analyses of fractures are available, except for fracture #11, and orientation data are based on core mapping only, cf. Table 4-1. The mineralogical description is based on macroscopic observations. The relative transmissivity of fractures could be addressed through flow tests in the section (cf. sections 3.4 and 3.5) and video imaging after drilling. Fractures #10 to #15 are studied in thin sections as well and the results are shown in Section 4.3.

By opening the borehole sections under short time period the connectivity with the neighbouring borehole KA3065A02 could be assessed. There may be a hydraulic connection of fracture #14 between both boreholes, which is also identified as the most probable (and only one) water conductive fracture in the 36-mm section in KA3065A03.

Table 4-1. Correlation of fractures between boreholes KA3065A02 and KA3065A03 based on macroscopic mineralogy and degree of openess. Ca=Calcite, Chl=Chlorite, Lau=Laumontite, Ep=Epidote, Pr=Prehnite, Myl=Mylonite, Fl=Fluorite, Ad=Adularia.

	KA3065A03		KA3065A02		
Fracture number	BH length strike/dip	Open/sealed	BH length strike/dip	Open/sealed	Comments
1	7.249 142/85	Sealed	6.38 150/85	Sealed?	Ca Ep
2	7.709 163/83	Open	6.96 336/86	Open	Chl Ca (ss)
3	8.329 147/66	Open?	Missing		Very thin Ca
4	8.779 141/86	Open	7.80 329/77	Open	Chl Ca +/-Lau
5	9.679 165/85	Sealed	9.14 143/79	Sealed	Ep,Ca +/-Pr
6	9.899 131/67	Open	8.82 318/82	Open	Ca,Chl (ss)
7	10.009 143/75	Open	9.06 156/81	Open	Chl, Ca, Claymin.
8	10.099 158/78	Sealed?	9.42 350/88	Sealed?	Ca Chl uncertain
9	10.209 326/85	Sealed	9.54 156/77	Sealed	Ca chl uncertain
10b	10.739 152/82	Open	9.88 152/82	Open	Observed only in core
10a	10.749 170/83	Open	9.89 156/88	Open	Myl. Ca,Chl
10c	Missing?		9.91 sub parallel to 9.96	Open?	Ca, Chl Observed only in core
10d	Missing?		9.96 176/76	Open	Chl, Ca
11	11.167 132/85.4	Weak indication Open?	10.33 323/79	Open?	Chl, Pr Observed only in core
12	11.347 310/79.6	Open, non conductive, Chl	10.54 330/88	Open? Non conductive	Chl, Ca
13	11.137 8.4/82.7	Sealed Ca, Ad Chl	10.57 185/80	Sealed Ca, Fl, Chl	Crossing, weak indication
14	11.637 338.4/54.2	Open, water conductive	10.80 308/56	Open, most probably water conductive	Ca, Chl Observed only in core
15	11.822 125.9/85.4	Open? Ca, Chl	10.92 322/71	Open?	Ca, Chl Observed only in core
16	11.327 315.9/84.6	Sealed Ca	Missing		
17	11.387 2.1/63	Sealed Ca,Lau	Missing		
18	11.427 6.3/67.8	Sealed Ca Lau	Missing		

An illustration of fractures with an interpreted correlation between boreholes KA3065A03 and KA3065A02 is given in Figure 4-1.

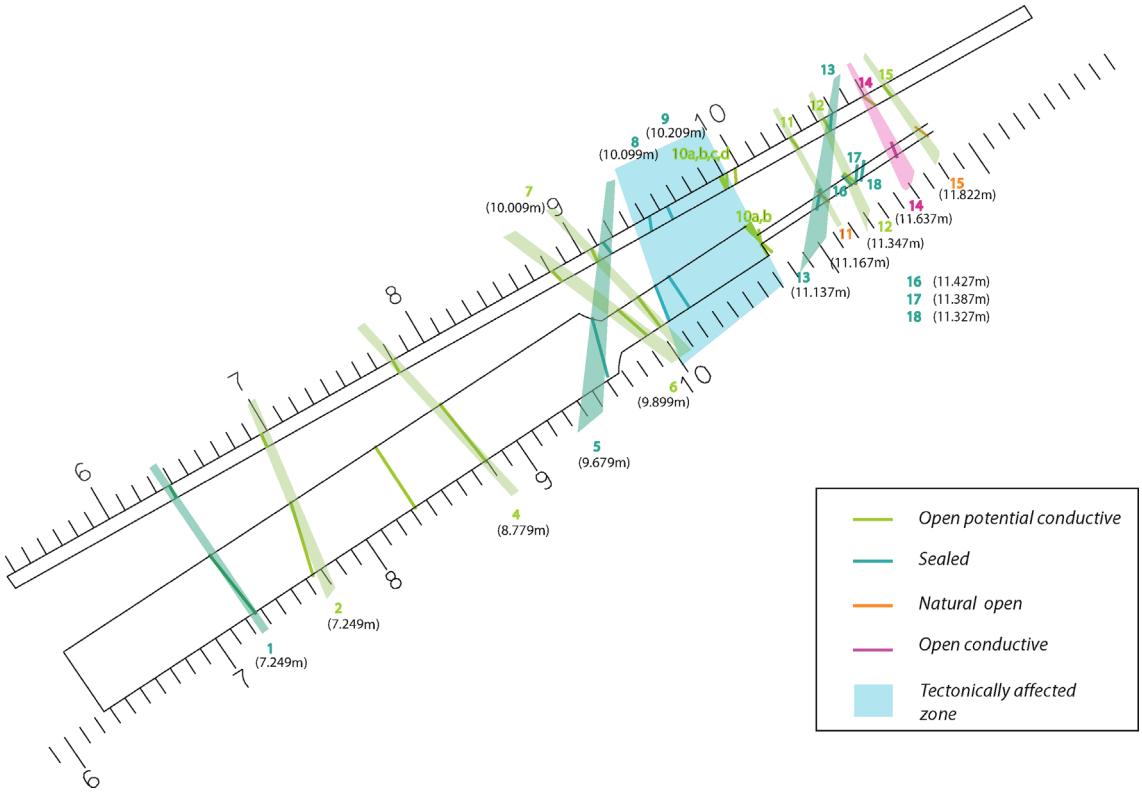

Figure 4-1 *Visualisation and interpretation of mapped fractures in boreholesKA3065A02 and KA3065A03, with potential correlation of fractures between the two boreholes. North is up in the picture, cf. Figure 3-6.*

4.3 Mineralogy and geochemistry

A detailed mineralogical study has been performed on fractures making up the target structure as well as fractures contained in the rock volume making up the intact rock section beyond the core stub. The fractures involved include #10 (the target structure), #11, #12, #13, #14 and #15. The studies are based on microscopy and SEM/EDS (Sweep Electron Microscopy and Energy Dispersive Scanning).

Some structures in the outermost part (< 9.5 m) of the boreholes were revisited and studied macroscopically. This information is contained in Table 3-1, cf. Section 3.1.

The results of macroscopic mineralogy and associated core observations are compiled in Table 4-1. As a result of this compilation some fractures were grouped together and it is suggested that they can be described and discussed as belonging to the same structure. The results of the microscopic mineralogy and geochemistry are compiled in Table 4-2.

Table 4-2. Detailed description of fracture intercepts based on microscopy and geochemistry.

Fracture	KA3064A03	KA3065A02	Comments
#10a and #10b	**10.739m (10b) and 10.749m (10a)** Fracture 10b has a coating of epidote, chlorite and calcite and indications of fault movements (slicken sides). Fracture 10a shows growth of idiomorphic quartz and calcite crystals as well as sulphide ($CuFeS_2$ grains). Some of the quartz crystals have cores of corroded fluorite. Small crystals of barite were identified. The mylonitic/cataclastic lense in between fracture 10a and 10b(5-17 mm wide) spans from pure epidote-quarts-albite-K-feldspar mylonite to cataclasite of tectonised and altered granitoid, probably Ävrö grainte. Biotite is replaced by chlorite, plagioclase is replaced by albite+epidote+sericite and quartz has recrystallised. One sealed fracture filled with adularia (low temperature K-feldspar) pigmented with ferric oxide/oxyhydroxide is observed parallel with the fractures 10**a** and 10**b.**	**9.88m (10b) and 9.89m (10a)** The fracture 10b coating consists of mainly calcite, chlorite and epidote and some minor grains of sulphides. The surface show clear mineral lineation indicative of fault movements. Fracture 10a shows a thin layer of calcite and chlorite. Also this surface show slicken sides. The lens between fracture 10a and 10b has a thickness of 7 –11 mm and consists of mylonite throughout, .	The structure can be explained as two parallel open fractures with a thin mylonic lens in between. Fracture 10b is the most water – conductive part of the structure. Fracture 10a constitutes the surface of the stub in KA3065A03. e.g. it will be the experimental surface for the nuclide sorption study. The lens between the fractures varies in thickness and composition but includes mylonite in both KA3065A02 and KA3065A03. Fractures #10 c and #10 d (splay fractures to the main fault) can not be found in borehole KA3065A03.
#11	**11.167 m** Very weak fracture indication. Presence of small amounts of clay. This is probably a fracture opened by the drilling. Red-staining and saussuritisation is observed in the wall rock but is likely related to #13 passing close by.	**10.33 m** Thin fracture coating with chlorite and calcite, traces of prehnite. Possibly open fracture. No obvious red staining is observed in the wall.	The indication in borehole A03 is very weak and this was first regarded as an artificial fracture, but the present interpretation is that it correlates to #11 in A02 and that this fracture fades out towards borehole KA3065A03.

#12	**11.347 m** This is a fracture with thin coating of chlorite and possibly some calcite. It is roughly perpendicular to the core axis. This fracture looks potentially open. One calcite sealed parallel fracture is found at a distance of 2 cm from #12 (11.327m). The wall rock is red-stained, saussuritised and the biotite is partly chloritised.	**10.54 m** Thin and a discontinuous layer of chlorite, calcite and minor grains of fluorite. The wall rock is red-stained and altered but some biotite grains are preserved. The fracture is potentially open and was judged as possibly conductive.	The two intercepts are very similar, both showing fracture coatings of thin (<50 μm) and discontinuous layers of chlorite. The wall rock is slightly altered in both boreholes. In borehole KA3065A02 the intersection is close to #13 showing significant wall rock alteration.
#13	**11.137 m** Several parallel thin, sealed fractures filled with laumontite, prehnite calcite and fluorite. The wall rock is significantly altered including albitisation, chloritisation and red-staining.	**10.57 m** Two parallel sealed fractures filled with prehnite calcite fluorite, (ortite?) and chlorite. The wall rock alteration is the same as for #13 in KA3065A03	Several sealed fractures filled with hydrothermal minerals found in a band of altered Ävrö granite showing saussuritisation and chloritisation. A similar and parallel band of alteration and sealed fractures are found in KA3065A03 with sealed fractures at core lengths of 11.387 m and 11.427 m.
#14	**11.637 m** Open probably water-. Conducting fracture coated with adularia and subsequent layer of calcite, fluorite and chlorite of spherulitic shape. Several sealed parallel microfractures are found in the wall rock. Wall rock alteration comprises saussuritisation but biotite is preserved	**10.80 m** Very thin discontinuous fracture coating of prehnite, adularia and chlorite. Wall rock alteration comprises saussuritisation but biotite is preserved	This fracture is much more evident in borehole KA3065A03 than in borehole KA3065A02 although together with #15 it forms a structure that is detected in both boreholes and it is probably of larger importance than earlier expected from observations in KA3065A02 alone.

#15	**11.822 m** This is the end of the KA3065A03 borehole. Only minor amounts of calcite coatings are found on the fracture surface. Quartz dissolution is observed close to the fracture surface. The biotite is altered to chlorite close to the fracture. Several thin, sealed fractures parallel with #15.	**10.92 m** The fracture coating consists of adularia, coated with calcite and spherulitic chlorite. The biotite is altered to chlorite in the wall rock close to the fracture. Grains of secondary allanite are also detected in the wall rock	The intercept of #15 in borehole KA3065A03 is very similar to the intercept of #14 in borehole KA3065A02. #15 and #14 are close (12-18 cm apart) and runs sub parallel.

Description of Structure #10 (the target structure)

Structure #10 is a reactivated fault with two roughly parallel fractures (#10a and #10b), just a few centimetres apart, and running through a mylonitic and cataclasitic central part of a ductile zone. The entire zone showing grain size reduction and red-staining are several dm wide. Fractures 10a and 10b are situated more or less along the border of the structure and in borehole KA3065A02 there are two splay fractures and an altered section of the rock reaching 7-8 cm from #10 a. It was the probably open splay fracture at 7 cm distance to 10a in KA3065A02 that was the real goal for the drilling of KA3065A03. As earlier described, however, this splay fracture was not found and the actual surface of the LTDE stub is 10a in KA3065A03. The prolonged borehole through the stub showed that the wall rock alteration is less extensive in KA3065A03 and only two very thin sealed fractures were found in the 2 centimetres beyond the stub. A weak red-staining reaches c. 10 cm into the rock from the stub surface.

It is worth pointing out that of the four intercepts of fractures 10a and 10b in KA3065A02 and KA3065A03, three shows slicken sides (both 10b intercepts and 10a in KA3065A02). The 10a intercept in KA3065A03 in contrast, does not show such indications. Pieces of the drillcore part corresponding to the stub surface have been used for thin section and SEM studies and it has been possible to distinguish the minerals grown on the fracture surface. The fracture is coated with chlorite, epidote and adularia with subsequent growth of idiomorphic crystals of quartz, calcite, chalcopyrite ($CuFeS_2$) and small grains of barite. Some of the quartz crystals are grown on corroded cores of fluorite. The size of the idiomorphic crystals are in the order of 50-100 µm. Figure 4-2 show SEM photos of quartz, barite and chalcopyrite.

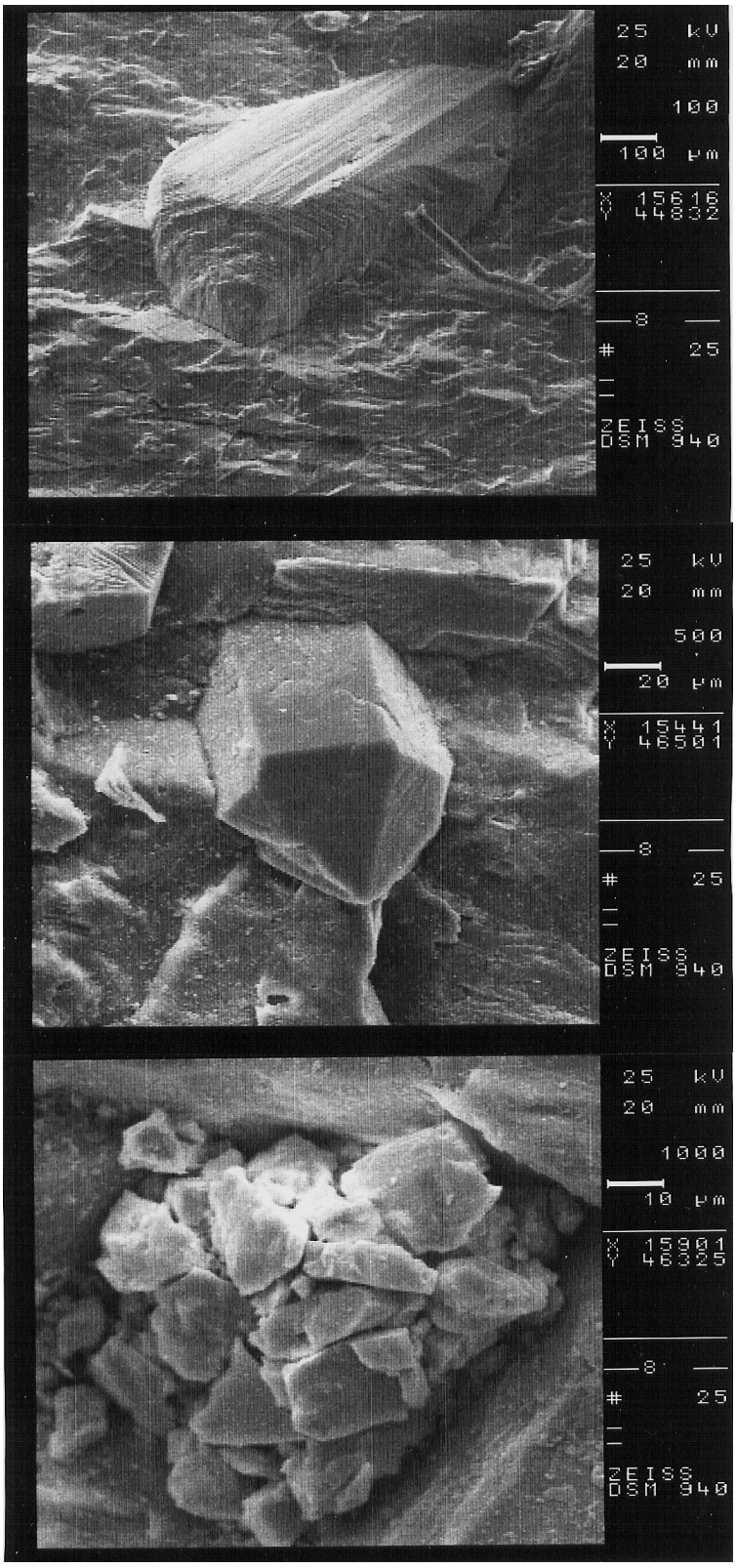

Figure 4-2. *SEM photo of chalcopyrite, $CuFeS_2$ (upper) , barite, $BaSO_4$ (middle) and quartz crystals (lower) grown on the #10a fracture surface in borehole KA3065A03 i.e. the surface corresponding to the stub surface in the borehole. Note the different scale bars (upper=100 µm, middle = 20 µm, lower=10 µm, cf. Table 4-2.*

One thin section has been prepared from KA3065A03 including fractures 10a and 10b and the mylonite/cataclasite in between. The mylonitic/cataclastic lense spans from pure epidote-quarts-albite-K-feldspar mylonite to cataclasite of tectonised and altered granitoid, probably Ävrö granite. Biotite is replaced by chlorite, plagioclase is replaced by albite+epidote+sericite and quartz has recrystallised. One sealed fracture filled with adularia (low temperature K-feldspar) pigmented with ferric oxide/oxyhydroxide is observed parallel with the fractures 10a and 10b The fracture surface of 10b is coated with epidote and extremely thin layers of chlorite and calcite. (Figure 4-3)

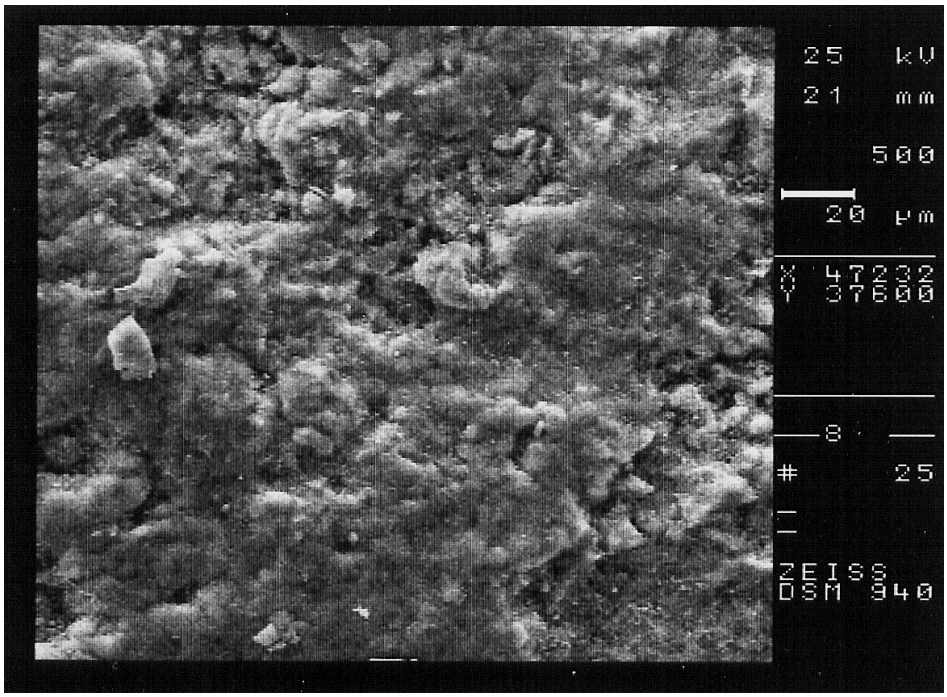

Figure 4-3. *SEM photo of the surface of #10b in KA3065A03 with calcite and chlorite grown on the fracture surface. The scale bar is 20 µm, cf. Table 4-2.*

Stable isotope analyses of the idiomorphic calcite on the target surface 10a in KA3065A03 has an uniform composition concerning $\delta^{13}C$ (-11.6 to –11.1 ‰ (PDB)) but show slightly more variation in $\delta^{18}O$ (–14.9 to –16.4 ‰ (PDB)). In borehole KA3065A02 the calcite of fracture 10a has a distinctly different stable isotope composition; $\delta^{13}C$ -13.9 ‰ and $\delta^{18}O$ –19.7 ‰.

The fracture 10b in borehole KA3065A03 shows large variation in $\delta^{13}C$ values (-10.4 and +12.3 ‰) of which the high positive value indicate *in situ* biogenic activity at some stage in the past. Also the $\delta^{18}O$ values show large variations (–20.0 and –13.3 ‰). Fracture 10b in borehole KA3065A02 shows $\delta^{13}C$ of –7.1 and $\delta^{18}O$ of –18.0 ‰.

A perpendicular thin calcite coated fracture (splay fracture) were also sampled and yielded values in good accordance with the idiomorphic crystals in KA3065A03 10a. The results are shown in Figure 4-4 together with all previously analysed fracture calcites from Äspö HRL.

Table 4-3. Stable isotope analyses of fracture calcites sampled from the cores of boreholes KA3065A03 and KA3065A02.

Borehole	$\delta^{13}C$ ‰ PDB	$\delta^{18}O$ ‰ PDB
Ka3065A03 : #10a 1	-11,5	-16
KA3065A03 : #10a 2	-11,7	-15,5
KA3065A03 : #10a 3	-11,2	-15,5
KA3065A03 : #10a 4	-11,1	-14,9
KA3065A03 : #10a 5	-11,6	-15,2
KA3065A03 : #10a 6	-11,6	-16,4
KA3065A03 : #10b 8	-10,4	-20,0
KA3065A03 : #10b 9	12,3	-13,3
KA3065A03 : #10 splay	-11,2	-14,9
KA3065A02 : #10a	-13,9	-19,7
KA3065A02 : #10b	-7,1	-18
KA3065A02 : #4	-12,3	-16,8
KA3065A02:#6	-14,6	-18,2
KA3065A03:#8	-12,2	-17,3

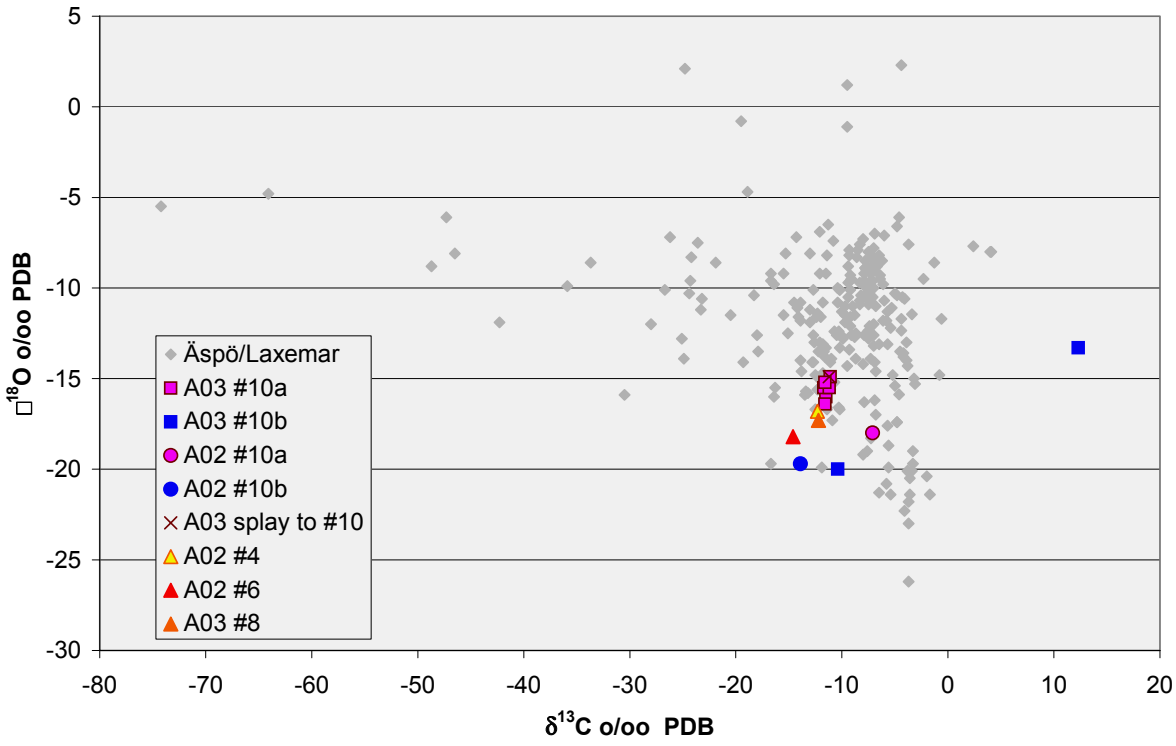

Figure 4-4. *Stable isotope data ($\delta^{13}C$, $\delta^{18}O$) for fracture calcites from the LTDE site compared with all other data from Äspö /Laxemar (cf. Bath et al., 2000).*

From the calcite analyses it can be concluded that calcite of different generations have precipitated in the different parts of the 10a and 10b fractures and the very low $\delta^{18}O$ values between -18.0 to -20.0 o/oo found in KA3065A02 10a and 10b and KA3065A03 10b**,** is typical for hydrothermal calcite precipitated relatively early in the geological history of the region. Such low $\delta^{18}O$-calcites usually have relatively high and uniform $\delta^{13}C$-values (-2 to -7 ‰). This is not the case here and the explanation may be that the calcite samples analysed are mixtures of different generations of calcites since the calcite coatings in these samples are very thin. The stub surface (KA3065A03 10a) deviates from this pattern in that it has a thicker calcite coating. The idiomorphic crystals from these coating have higher $\delta^{18}O$ values supporting a probably lower temperature (and younger age) for the growth of these crystals. Higher $\delta^{18}O$ are also detected in the samples (KA3065A03 10b) with the extremely high $\delta^{13}C$-value (+12.3 ‰ PDB) indicative of bacterial activity in the past.

The aim of the study of fracture10 is, besides getting information for characterisation and correlation of the structure, to describe the surface of the core stub. It should be kept in mind that there are variations in the degree of calcite and quartz coverage on the surface. However, based on the videoscope observations of the stub surface there is a relatively good correspondence between the stub surface in KA3065A02 and its counterpart in the borehole KA3065A03. This means that the minerals found in the investigated samples of fracture 10a are expected to be found also on the surface of the core stub. These minerals are, in addition to calcite and chlorite; quartz, chalcopyrite, fluorite, barite, epidote, adularia (low-temperature K-feldspar). A simplified sketch of the target surface on the core stub is shown in section in Figure 4-14.

Description of Fracture #11

One sample of the coating of fracture #11 in KA3065A02 has been compared with a similar sample from #11 in KA3065A03. In borehole KA3065A02 the fracture is coated by chlorite and small idiomorphic grains of calcite. It is not possible to determine if this was an originally open, semi-open or sealed fracture. In borehole KA3065A03 however, the fracture indication is very weak. The core is broken and it was initially regarded as an artificial break but after observations using stereomicroscope, some indications of a potentially natural fracture surface was observed. Studies using SEM/EDS support the presence of a possible natural fracture. It looks like there is a natural fracture plane sub-parallel with the studied surface (breakage?) and there are minor amounts of clay minerals found at one spot along the fracture interception (cf. SEM photo Figure 4-5). The rock is more hydrothermally altered in this section of the bedrock and plagioclase show signs of albitisation.

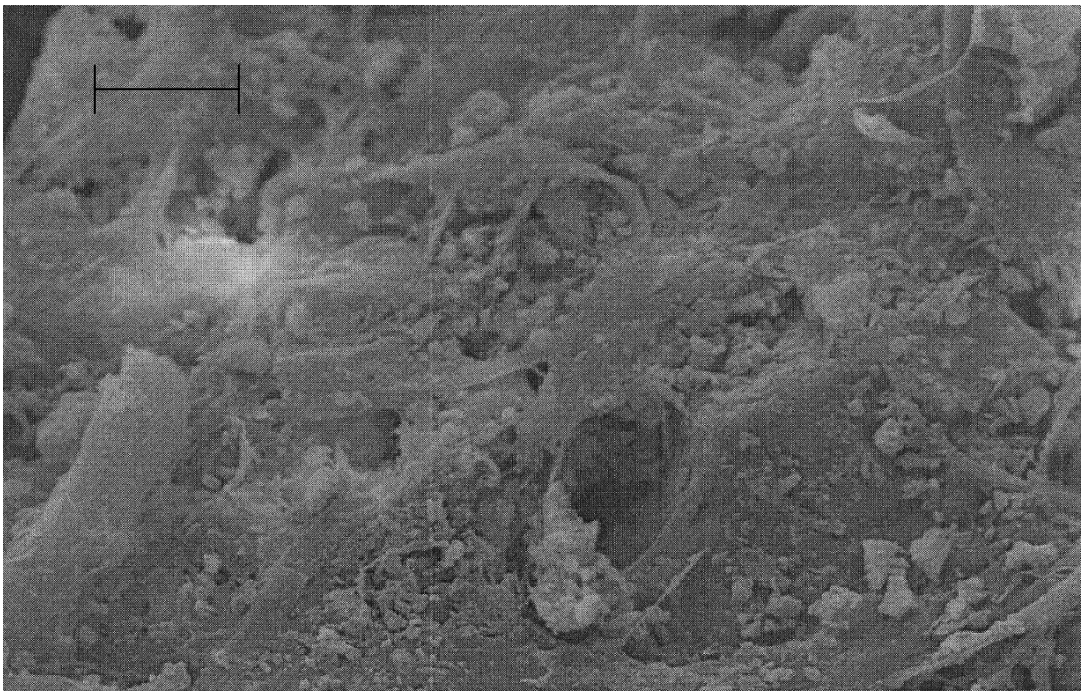

Figure 4-5. *SEM photo of #11 in borehole KA3065A03; small flakes of clay minerals on the rough fracture surface. The scale bar is 20 μm, cf. Table 4-2.*

In conclusion the interpretation of fracture #11 is still somewhat uncertain. One possibility is that #11 fades out towards KA3065A03 and that the weak indication in KA3065A03 is located close to the termination of the fracture. Support for this hypothesis includes:

- The orientation of fracture #11 in KA3065A03 fits well with the extrapolation from KA3065A02 of the corresponding intercept (as obtained from BIPS)
- The small spots with alteration products (clay minerals)
- The fracture sub-parallel with the breakage.

On the other hand;

- The fracture minerals present on the surfaces of fracture #11 in KA3065A02 (chlorite and calcite) are not found in KA3065A03.
- The breakage is hosted in an altered part of the bedrock and this may partly explain the presence of secondary minerals.

For the purpose of the LTDE experiment it is, however, wise to note the possible presence of a fracture #11 and therefore it is included in this compilation.

Description of Fracture #12

This fracture is roughly (almost?) perpendicular to the core axis of both boreholes and is characterised by a thin and discontinuous layer of chlorite, and in places calcite. The fracture is evident in both boreholes with equal weight. The wall rock is sausuritisised close to the fracture edges and the biotite is partly altered but is not replaced.

A parallel calcite-filled fracture denoted #16 in KA3065A03 (missing in KA3065A02) some 2cm away can probably be connected to fracture #12.

The red-staining and alteration that appears in the vicinity of #12 in KA3065A02 seems to be more related to fracture #13.

The intercepts of #12 in KA3065A02 and KA3065A03 are regarded as open and possibly water-conducting, however, the performed hydraulic tests did not provide evidence that this fractures is conductive.

Description of Structure #13

This is a c. 5 cm wide band of altered and red stained rock including several sealed, thin, parallel fractures filled with hydrothermal minerals like prehnite, laumontite and fluorite and calcite (poor in manganese) and chlorite. The wall rock alteration comprises chloritisation, albitisation and precipitation of small hematite grains causing the red-staining. In KA3065A02 one of the fractures has voids (due to dissolution of quartz and/or calcite) in the order of 100 μm.

Structure #13 is orientated NNW in contrast to the otherwise for the most part NE – ENE striking fractures in the inner part of the boreholes.

Two sealed fractures denoted #17 and #18, at L=11.387 m and L=11.427 m, respectively, in borehole KA3065A03 are similar in style and orientation to #13, although the alteration is less extensive. These two fractures are missing in KA3065A02 but the BIPS images indicate bands of red-staining with the same orientation at a corresponding depth in KA3065A02.

In conclusion, it is suggested that fracture #13 consists of several 1-5 cm wide, NNW trending bands characterised by significant hydrothermal alteration (including Fractures #17 and #18). Several sealed fractures are contained within these bands.

Description of Fractures #14 and #15

Fractures #14 and #15 are two sub-parallel fractures located at an interdistance of 18 cm in borehole KA3065A02 and 12 cm in KA3065A03, cf. Table 4-2. In borehole KA3065A02, fracture #15 is the more prominent of the two and this intercept is very similar to fracture #14 in borehole KA3065A03. It is however, not possible, based on available data, to determine whether this really is the same fracture. Therefore it is suggested that fractures #14 and #15 are regarded as part of the same structure (including several sub-parallel open and sealed fractures).

The fracture coatings are adularia, spherulitic chlorite, fluorite and calcite. Small spots of REE-carbonate have been detected with SEM. The wall rock shows saussuritisation, and biotite is altered to chlorite in the immediate vicinity of the fracture edges. Allanite and epidote were also detected in the wall rock close to the fracture.

The structure containing fractures #14-#15 is probably more evident than initially expected based on results from KA3065A02 alone. The only significant hydraulic response in the slim-hole part of borehole KA3065A03 was detected in this structure is attributed to fracture #14.

4.4 3D model of fracturing

A 3D model of the interpreted fractures in KA3065A03 and KA3065A02 is presented in Figures 4-6 and 4-7.

The 3D model is constructed on the basis of fractures identified from BIPS 4 measurements in KA3065A02 and KA3065A03 (196.5-mm part), and on fractures mapped in core for the 36-mm section of KA065A03.

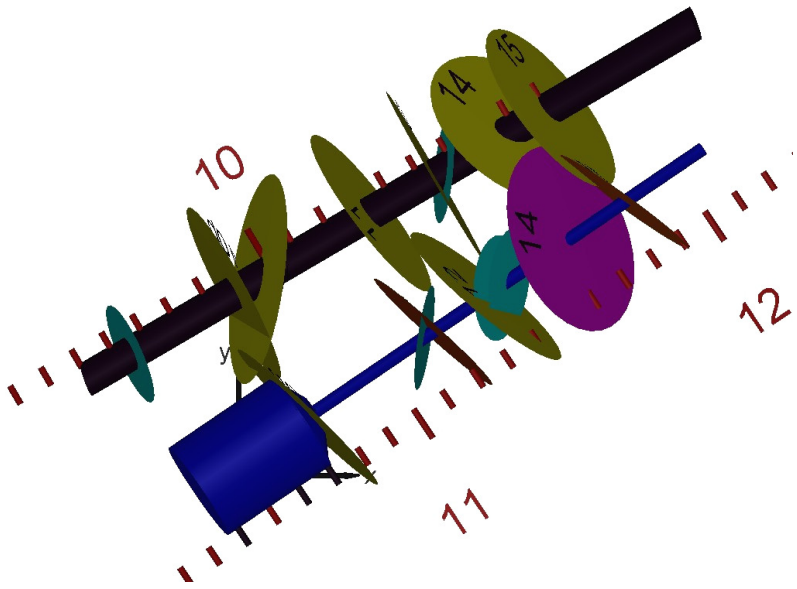

Figure 4-6. *3D model of the 36-mm section of KA3065A03 (blue outline) and corresponding depth in KA3065A02 (brown outline). The different colours of the fractures are related to the correlation as illustrated in Figure 4-1. North is up in the picture, cf. Figure 3-6.*

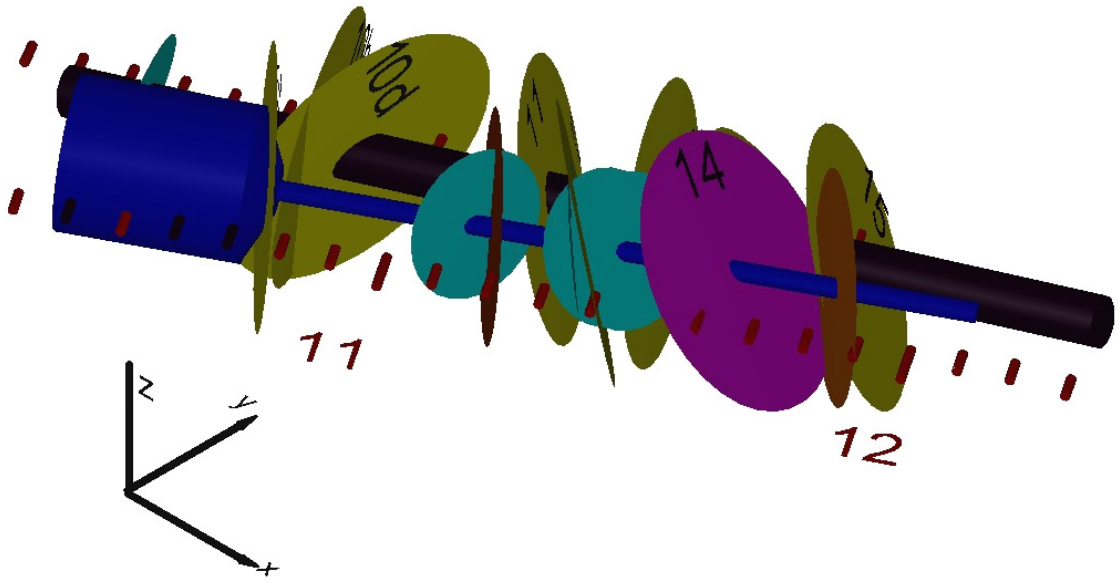

Figure 4-7. *3D model of the 36-mm section of KA3065A03 (blue outline) and corresponding depth in KA3065A02 (brown outline). The different colours for the fractures are related to the correlation as illustrated in Figure 4-1. (y= North; x= East)*

4.5 Physical description of core stub surface

The face of the stub at approximately 10.24 m depth in KA3065A03 is an irregularly sub-planar fracture surface almost orthogonal to the borehole axis, cf. Figures 3-5 and 4-1, closely coupled to the main fault as observed on the borehole wall around the stub, c.f. Figures 4-8 through 4-10. The fracture surface appears to have lost a piece of the upper left corner. This is interpreted as being a result of a minor fracture intersecting at an oblique angle to the target structure. Despite its apparent planarity, the surface has a somewhat uneven surface with its centre part slightly higher than the surrounding. Two types of measurements, manual (Figure 4-11) and laser scanning (Figure 4-12) reveal the roughness of the surface in detail. The absolute measures of the position of the surface are best surveyed with a total station (directly reflective). However, this method does not cover the whole surface due to reflections in the borehole wall, and cannot accurately reveal the intersecting fracture in the upper left corner. The two measurements have been merged into the illustration of the fracture surface given in Figure 4-10. In order to improve the interpretation of the surface of the stub a plaster cast (in a latex liner) of the stub surface has also been made. Figure 4-10 also shows the geological characteristics of the fracture surface as well as a simplified illustration of the geology (stratification) in the main fault as observed through the video images taken from the borehole. Calcite and chlorite fillings cover the major part of the target surface. Small patches of the surface reveal the underlying Äspö diorite.

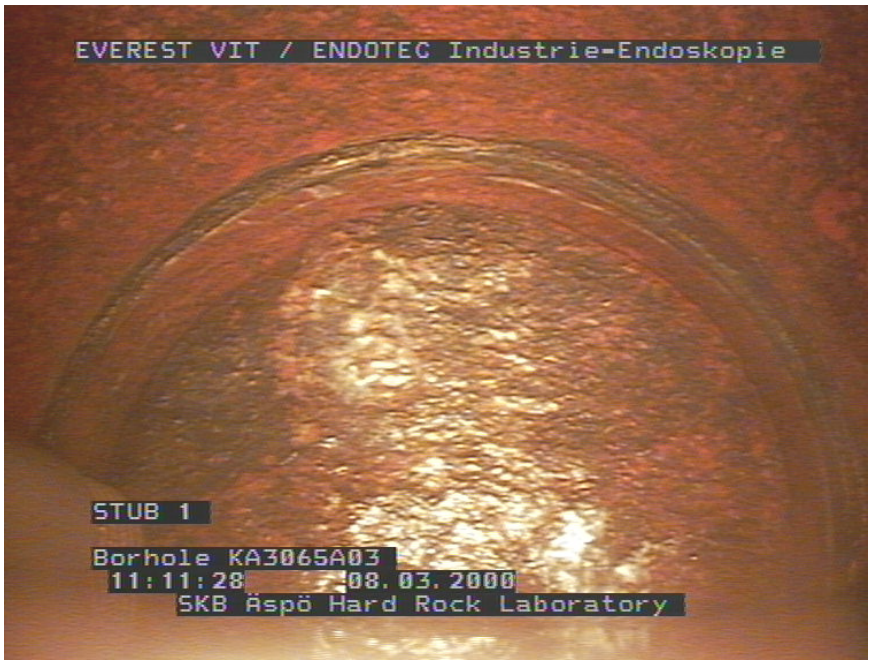

Figure 4-8. *Image of the target fracture surface. Still from the ENDOTEC video. The greenish band that surrounds the circumference is the main fault that was penetrated before the target fracture. The white area on the surface is calcite and the green is mainly chlorite. There is an intersecting fracture that has cut a part of the fracture surface in the top left corner.*

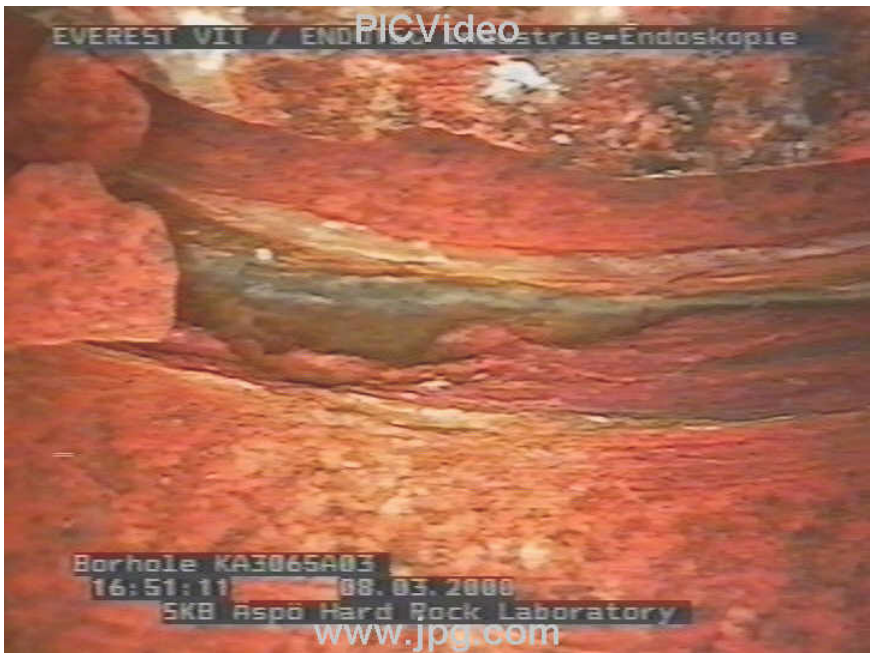

Figure 4-9. *Detailed image of the lower circumference of the borehole and the lower part of the stub. The coloured band in the main fault consists of epidote, chlorite and calcite. The entry to the slot is readily visible in the upper part of the image as a dark curved band. In the left side of the photograph, loose cm sized fragments are readily identified on the bottom of the borehole and partly covering the entry to the slot.*

Video images of the wall of the stub show that the diorite is not deformed or altered. The opposite part of the face of the stub is covered by a mm thick layer of calcite, as can be inferred from the circumference of the borehole wall as well as from pieces of the matching "outer" surface of the fracture, c.f. Figure 4-3. Finally, Figure 4-14 shows a perspective 3D view of the stub and its surface.

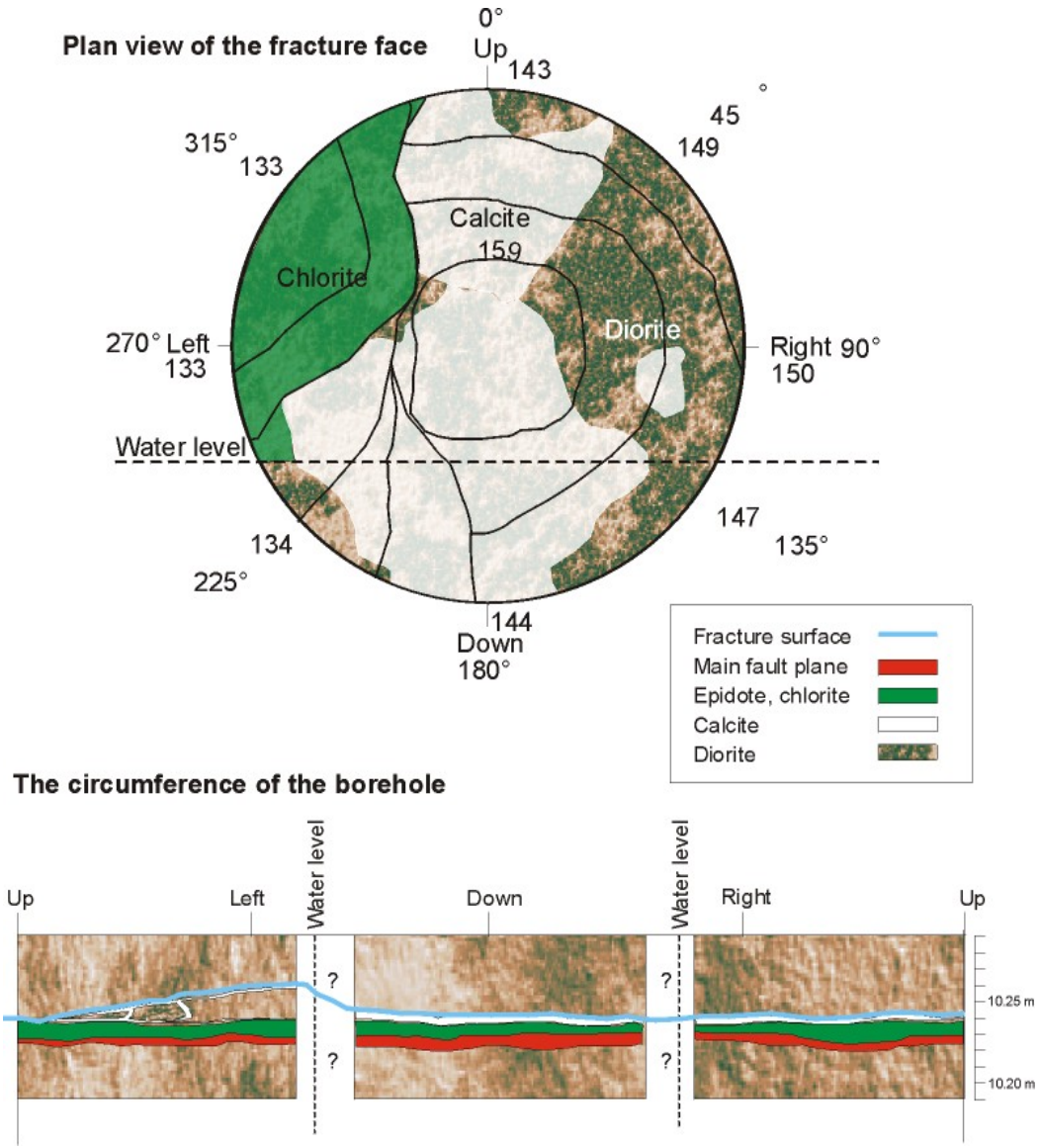

Figure 4-10. *Illustration of the face of the target fracture and the circumferenc of the target structure around the borehole. The hatched line indicates the part of the face that was covered by water during the inspection. The illustration shows a combination of the results from video and still images from the ENDOTEC and Pierpoint video systems. The surface topography is a combination of video, total station and the measurements with plastic ruler. The values given along the circumference shows the length of the stub in mm using the borehole bottom (L=10.40 m) as a reference datum.*

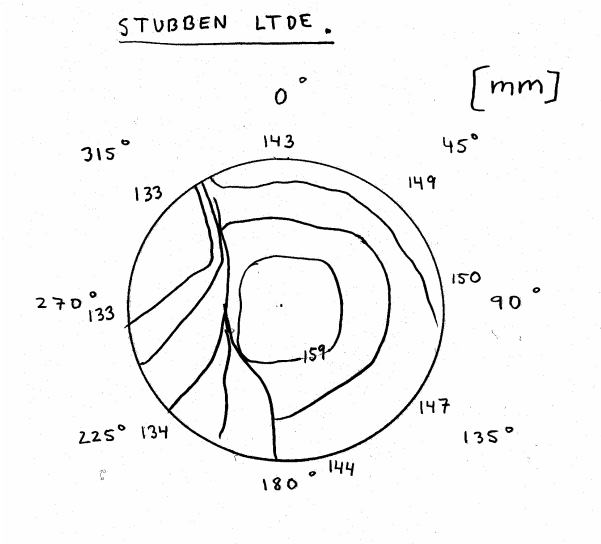

Figure 4-11. *Illustration of the manual measurements of the geometry of the stub surface. The measurements are made with a plastic ruler that has been inserted into the hole and onto the fracture surface. Indicated depths use the borehole bottom (L=10.40 m) as their reference datum.*

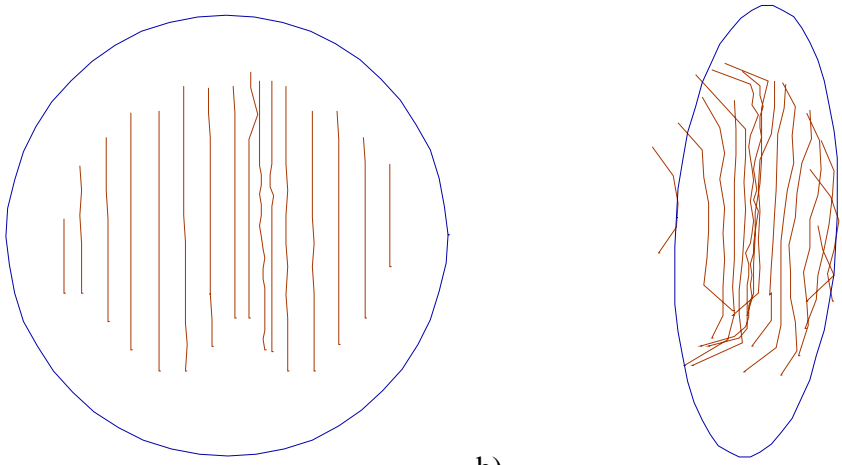

a) b)

Figure 4-12. *Illustrations of the laser scanning measurements of the fracture surface in two different angles, A and B. The surface is scanned in sections (orange lines) surrounded by a 196.5 mm borehole periphery (blue circle). The equipment does not allow proper measurements close to the borehole wall as shown in Figure 5-2a. This effect is seen clearly in Figure 5-2b where the measurements are deflected closer to the periphery.*

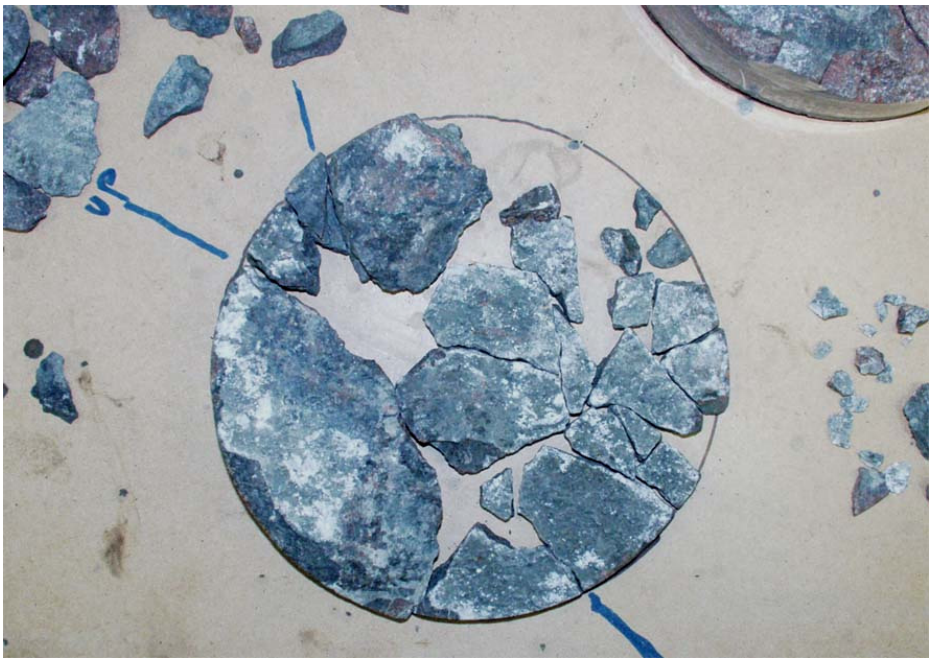

Figure 4-13. *The matching surface to the target fracture. The major part of the surface is covered by a mm thick layer of calcite as can be inferred from the borehole wall next to the stub. The main fault is extensively deformed and shows strike slip behaviour.*

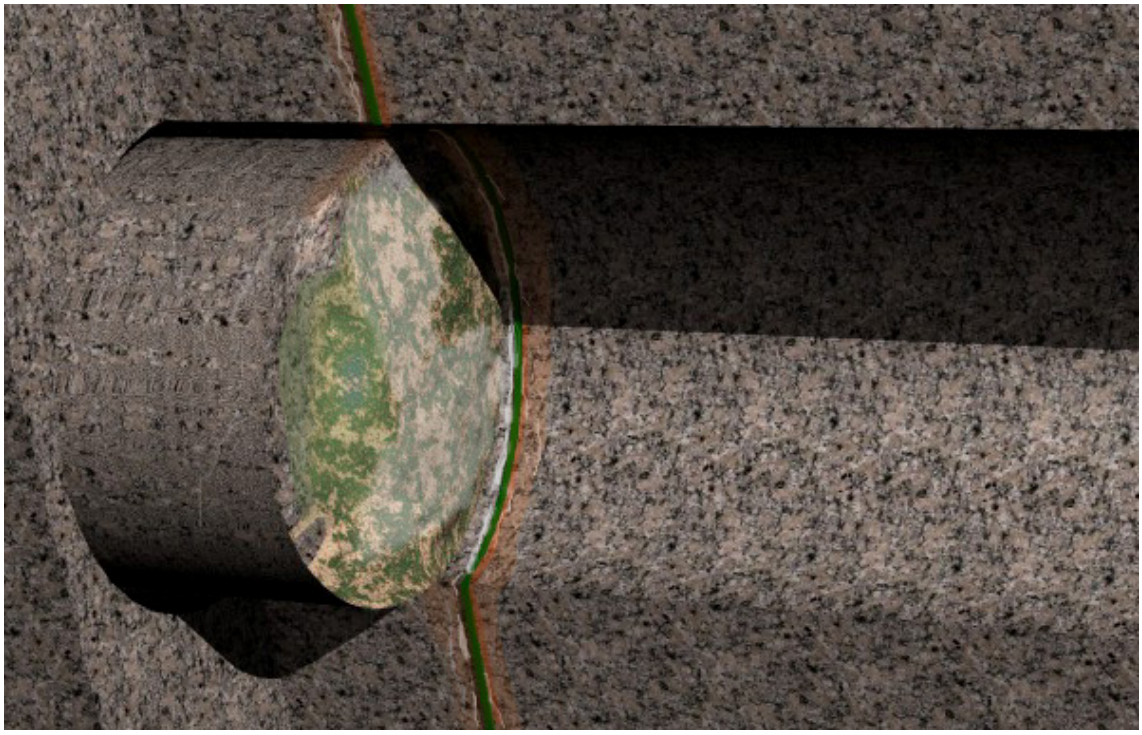

Figure 4-14. *Illustration of the stub and the location of the fault on the borehole wall. The surface is covered by calcite (white) and chlorite (green). The upper left part shows the surface of the chlorite-covered splay fracture intersecting the main surface. The main fault is shown as the red-green-white altered epidote and calcite filled section of the rock.*

4.6 Geology and mineralogy of matrix of intact rock section

The most suitable section of intact rock for the planned diffusion experiment is the section from L=10.8 to 11.1 m in the inner slim hole part of KA3065A03.

The stub surface is found at L=10.749 m and a red-staining and alteration associated with the target fracture #10a reaches some centimetres into the drillcore but from L=10.8 m a relatively fresh granodiorite with a few K-feldspar porphyroblasts (approximately 1 cm in size) constitutes the wall rock. A weak foliation is orientated approximately 45^{o} to the core axis. At L=10.9 m a small aggregate of hornblende is present as a black spot ca 1 cm in size.

At L=11.0 to 11.15 m the granodiorite becomes more evenly grained and the plagioclase crystals are successively more altered, and the rock more red-stained when approaching fracture #13 at L=11.13 m.

Mineralogically, the rock consists of plagioclase (partly saussuritisised), K-feldspar, quartz and biotite. Accessory phases consist of magnetite, titanite, zircon and apatite. Secondary minerals like epidote, sericite and some chlorite and fluorite are present throughout the drill core.

5 Assessment of sample disturbance

It is expected that some element of disturbance will affect the peripheral parts of the rock cylinder that makes out the remaining stub in the borehole. The original objective was to obtain a 50 mm stub at the bottom of the borehole with the target structure at its face. Given the projected diffusion depths which have been projected to be in the order of a few decimetres the majority of the diffusion would be in the intact matrix rock beyond the stub. The drilling of the experimental borehole resulted in a stub of 150 mm length, ie. a 3 times longer stub than originally planned. This entails that a larger portion of the diffusion length would be in the stub itself if an experiment was made in the stub. This puts a high demand on the assessment of the degree of damage in the stub.

Based on previous studies, there are five main factors which affects the bottom hole stress concentration, and thereby the fracturing of the core (Hakala, 1999);

1) The in-situ state of stress relative to the borehole orientation
2) Drilling-induced loads
3) Bottom-hole geometry
4) Properties of the rock
5) Pore pressure

In the following, a couple of independent studies are accounted for which forms the basis for assessing the sample disturbance exerted on the stub in the bottom of borehole KA3065A03. The studies are mainly focused on aspects related to items 1 and 4, and partly to items 1 and 3.

5.1 Sample disturbance due to drilling load and hole bottom geometry

The drilling induced loads have a direct effect on the state of stress in the immediate vicinity of the borehole bottom and therefore affect the fracturing of the core. The drilling-induced loads comprise of a borehole-aligned load transmitted via the drill bit, the rotational shear force on the drill bit-rock interface, and the pressure of the drilling fluid. It has been assessed that the magnitude of the axial load is in the order of 10 MPa, whereas the shear force is approximately 50% of the axial load (Hakala, 1999).

Another component that defines the redistribution of stresses close to the borehole bottom is the geometry of the borehole bottom itself. The ratio between cut widths to core diameter has minor effect, but the shape is more critical. Being flat, rounded or V-shaped cutting edge may have almost 100% effects on the stresses near the drill bit (Li, 1997). Generally, a rounded cutting edge produces lower stress concentrations.

In the case of the drilling of KA3065A03 a flat cutting edge was employed.

5.2 Rock-mechanical assessment of stress-induced fracturing

No specific rock mechanical analysis of stress-induced fracturing has been performed within the context of this study. Instead the results of Hakala (1999) have been used and translated to the situation applicable for borehole KA3065A03. However, new analysis of stress mode with geometries applicable to KA3065A03 is reported in Section 5.5.

In general, the tunnel and the investigation drift, located some 10 meters away from the target feature in KA3065A03, are assumed to have minor effect on the orientation and magnitude of the *in situ* state of stress. Hakala (pers. comm) consider the effect to be in the range of 10%. Given this, the principal *in situ* stresses and other relevant parameters can be inferred from stress data and materials tests, as given in Table 5-1.

Table 5-1 . Inferred rock mechanical data applicable to the situation near KA3065A03.

Parameter	Magnitude
Horizontal principal stress $\sigma_H = \sigma_1$	25 MPa
Horizontal principal stress $\sigma_h = \sigma_v = \sigma_2$	10 MPa
Horizontal principal stress $\sigma_v = \sigma_3$	5-10 MPa
Tensile strength σ_t	16 MPa
Uniaxial compressive strength σ_c	195 MPa
Poisson's ratio	0.25
$\sigma h / \sigma H$	0.2-0.4
$\sigma v / \sigma H$	0.4
$\sigma t / \sigma H$	0.6
Hoek-Brown failure criteria *mi*	12

All assumptions made by Hakala are fulfilled with the exception of the Hoek-Brown failure value *mi* and the borehole bottom geometry. The value of *mi* assigned to Äspö diorite may appear to be on the low side. In the assignment a value of 25 was considered high, whereas a value of 7 was considered low. There is consequently a possibility that the failure mode can deviate from a clear tension fracture. With regards to the borehole bottom geometry, cf. Section 5.1, the slot width normalised to the core radius in Hakala's study is (56-42)/42=0.33, whereas for the inner part of KA3065A03 the value is (197-177)/177=0.11. Li (1997) has reported a relatively small effects of this ratio but it is considered that a lower ratio will produce less damage, or damage with shorter extent, relative to the core diameter (Hakala, pers. comm.).

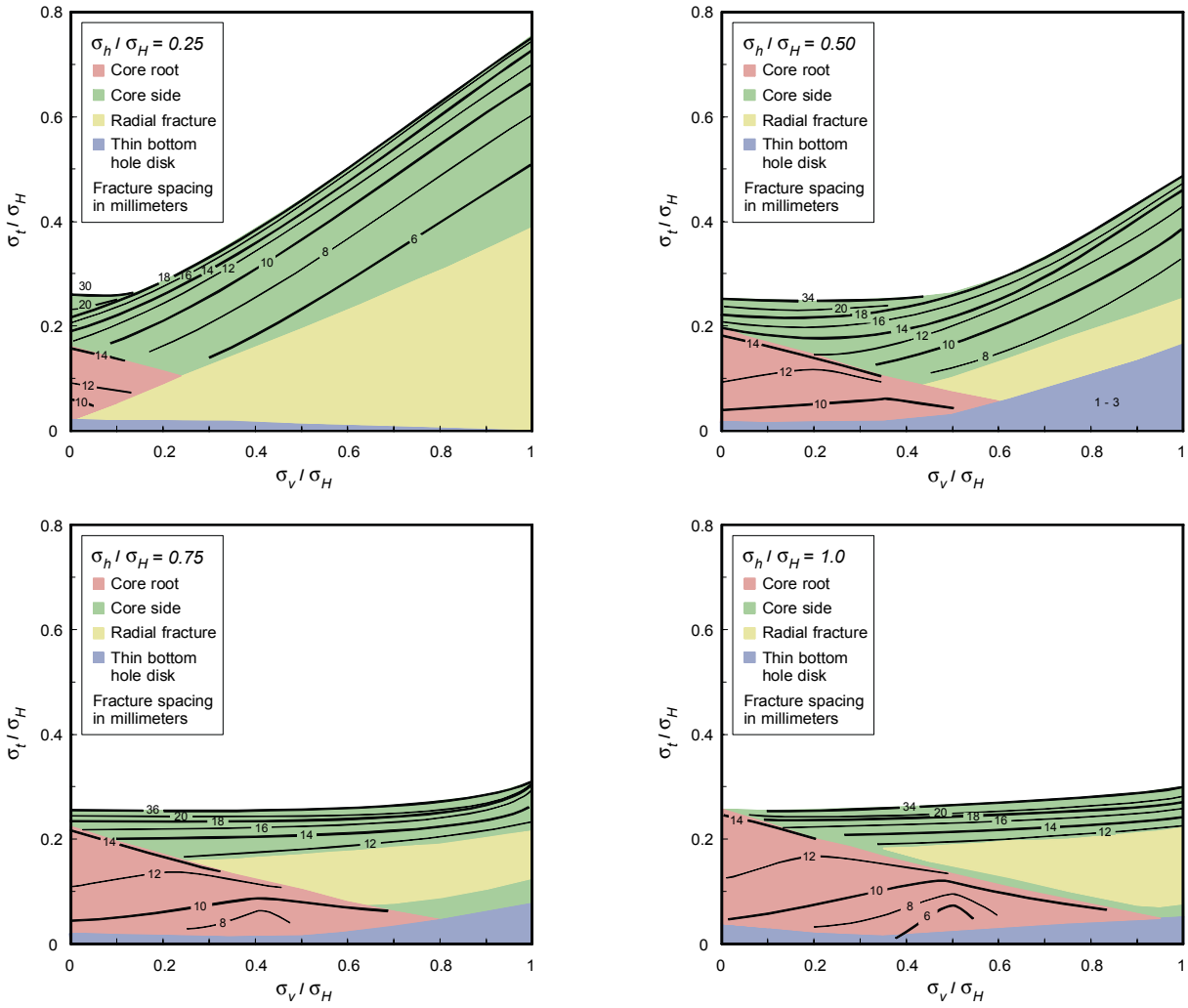

Figure 5-1. *In situ stress interpretation nomogram - Fracture spacing and fracture initiation point in normal coring situation (Borehole dimension = T56), Posson's ratio = 0.25 (Figure 9.1 in Hakala 1999).*

With the above parameters fixed and making use of the nomogram-type figures produced by Hakala (1999), cf. Figure 5-1, no core damage in terms of developed new fractures is to be expected. Although no induced new fractures are expected, the following aspects may promote fracturing; 1) drill bit pressure during the coring (Section 4.1), 2) rotation of the *in situ* stress field, 3) deviation in, or exactness of material parameter values in Table 5-1.

Figure 5-2 presents an interpretation nomogram for the extent and shape of fractures induced under normal coring conditions. Hakala's (pers. comm.) interpretation of Figure 5-2 is that induced new fractures visible to the eye are only seen in the yellow, red and ´"thin-bottom hole disk" stress-strength ranges. The cyan and blue areas are for stable, short extent fractures that are for the most part not visible to the eye, and instead PMMA impregnation or electron microscopy are required. The green area is more of a transition zone between stable/unstable fracture growths. The grey area is a bit complicated, the maximum tension is tangential producing radial fracturing, but with advancing coring also unstable root or side-initiated fracturing may occur.

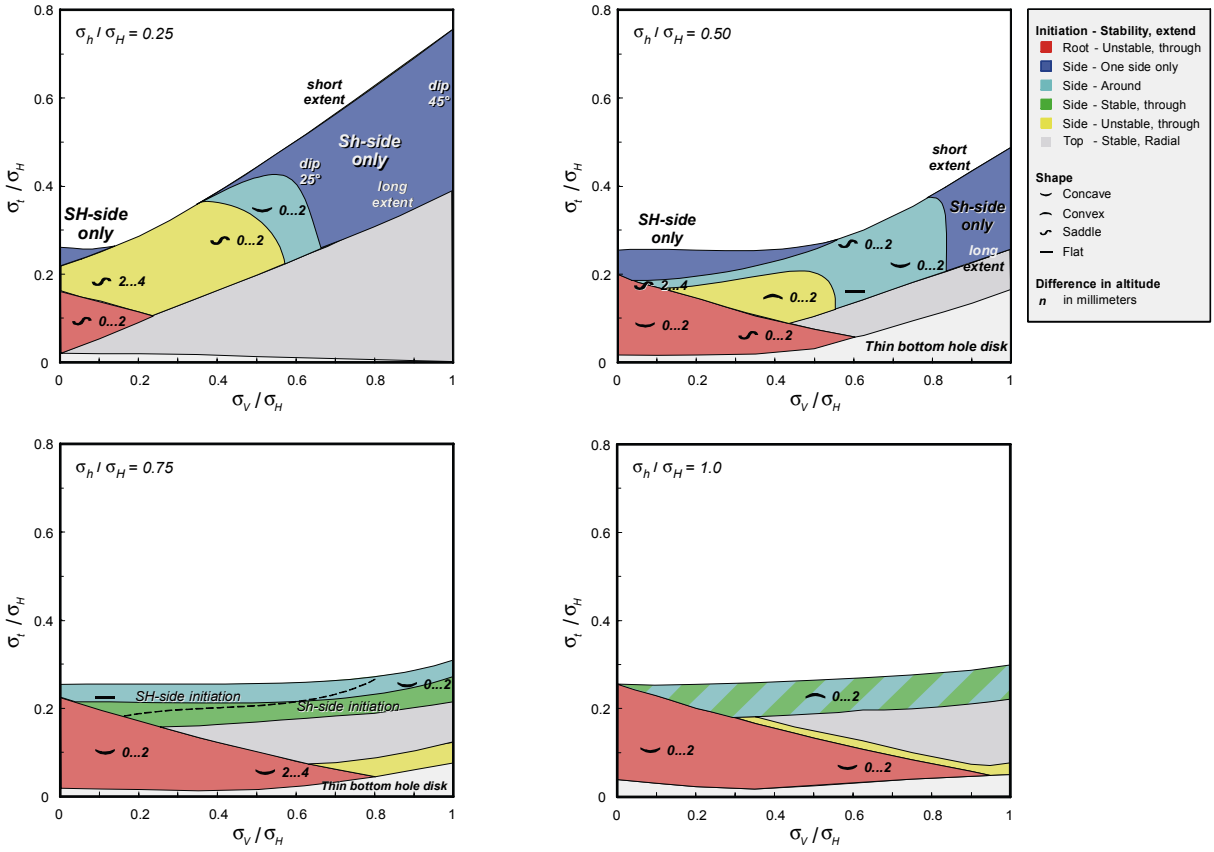

Figure 5-2. *In situ stress state interpretation nomogram – Fracture initiation point, stability, extent and shape in a normal coring situation (Borehole dimension = T56), Posson's ratio = 0.25 (Figure 9.3 in Hakala 1999).*

Hakala (pers. comm.) also identifies that none of the primary loads produces the high radial tension needed to produce tangential fracturing. Undoubtedly, radial relaxation will occur which will allow opening of already existing tangential micro-fractures, but relaxation will happen in all directions.

In conclusion, the borehole geometry in relation to the assumed present stress state, the assumed material properties and the loads induced during drilling are not assumed to cause development of newly formed micro fractures. However, the imposed relaxation of the stress state resulting from the coring may result in widening of existing fractures irrespective of their orientation.

5.3 Seismic assessment of sample disturbance

A study has been performed with the aim of assessing the degree of disturbance (mechanical damage and disturbance due to stress redistribution) using measurements of seismic P-wave wave velocity across the diameters of cores. The measurements have been performed on two types of core material; 45 mm material from a section in KA3065A02 (L=9,4 m to 10,33 m) including the mylonitic marker horizon. In addition measurements were made on a 25 cm piece of the 177 mm core from KA39065A03.

The latter section is located approximately between L= 10.20- 10.45 m, ie. approximately 0.25 m from the target structure. In both cases measurements were made across the core diameter along two orthogonal sections along the core.

The results of the measurements on the 45 mm core specimens from KA3065A02 indicates an average P-wave velocity of 5550 m/s, cf. Figure 5-3.

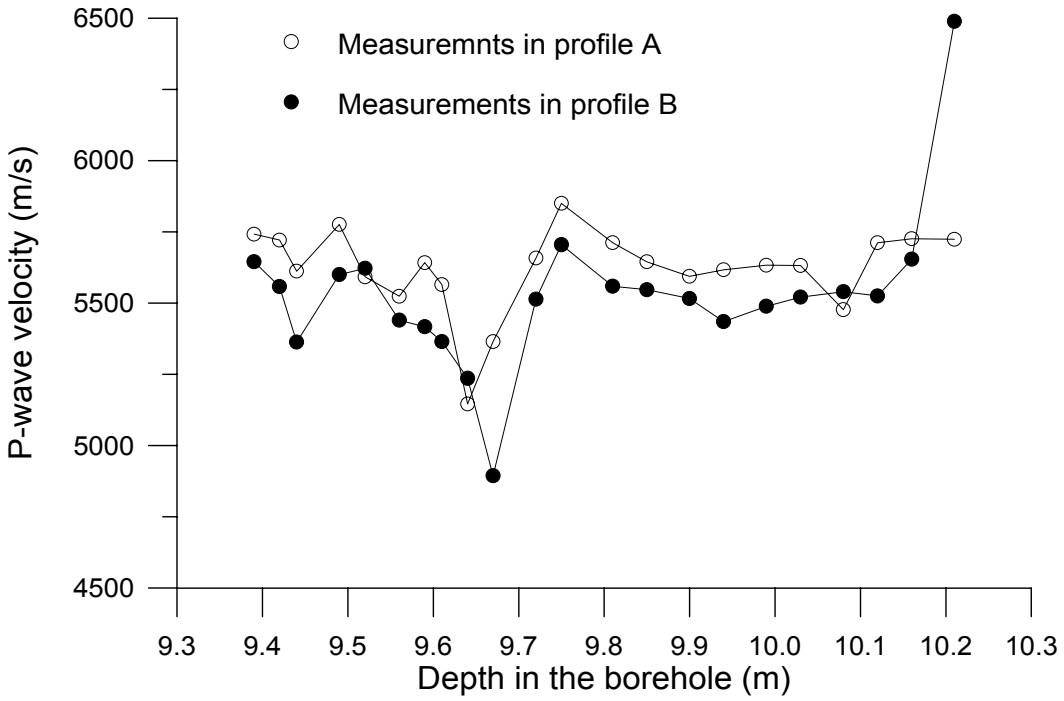

Figure 5-3. *The P-wave velocity at the measurement points on the 45 mm core specimens from KA3065A02. The extreme value at the upper right of the figure was omitted in the calculation of the average value (length coordinates measured from rock surface).*

The results on the 177 mm core indicates an average P-wave velocity of 5780 m/s, cf. Figure 5-4.

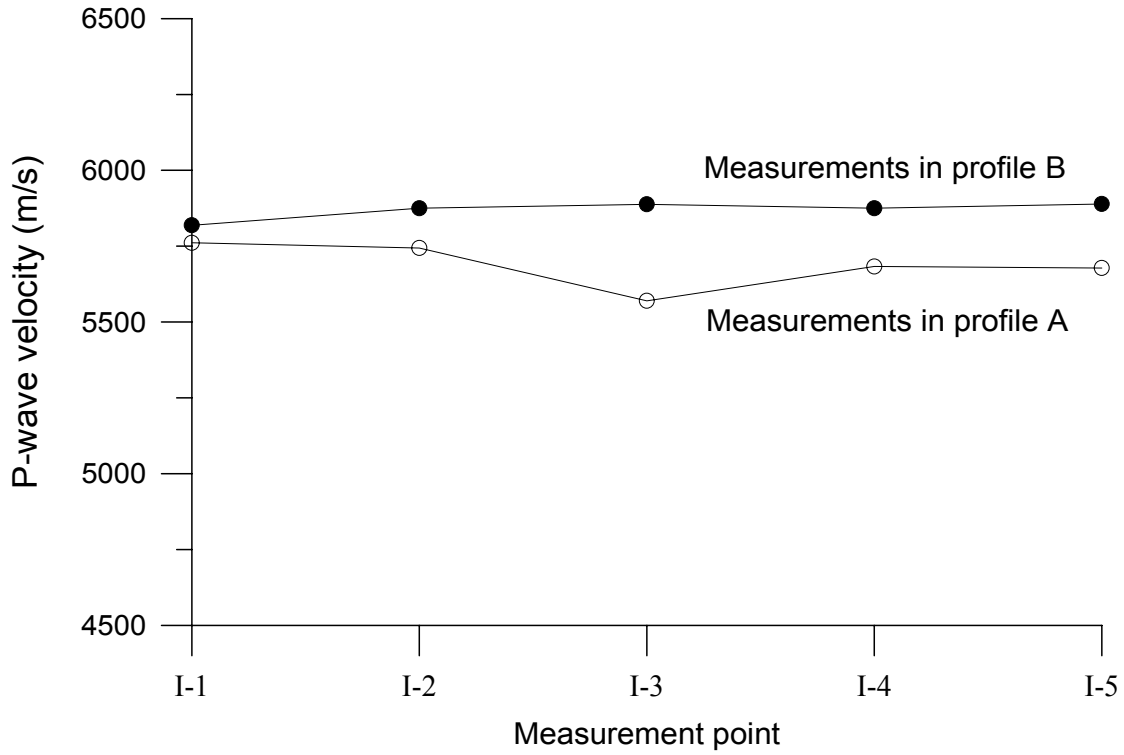

Figure 5-4. *The P-wave velocity at the measurement points on the 177 mm core specimens from KA3065A03. The extreme value at the upper right of the figure was omitted in the calculation of the average value.*

It is seen in Figure 5-3 that the P wave velocity in the ϕ45 mm cores from KA3065A02 decreases monotonically from 9.39 m to 9.67 m, both in profiles A and B. This reduction in the P-wave velocity may be caused by the geological structures and texture. In specimens located at 9.67 and 6.72 m respectively, we could see an obvious joint filled with soft material.

It is shown in Figures 5-3 and 5-4 that the P wave velocity in the two orthogonal profiles A and B, both in the ϕ45 mm and ϕ177 mm specimens, are slightly different. This may be owing to the geological anisotropy of the rock. In the ϕ45 mm cores the average P wave velocity is about 5620 m/s (profile A) and 5480 m/s (profile B). The difference in the P wave velocity between these two orthogonal profiles is 140 m/s. In the ϕ177 mm core the average P wave velocity is 5690 m/s (profile A) and 5870 m/s (profile B). The difference in the P wave velocity in this case is 180 m/s. Therefore, it can be stated that the geological anisotropy in the rock may causes a reduction of 140 m/s to 180 m/s in the P wave velocity when the measurement plane is rotated 90 degrees.

Considering the relatively large diameter of the ϕ177 mm core from KA3065A03, it is logic to say that the ϕ177 mm core specimen was little or not damaged during the process of over-coring. The overall average P wave velocity of the ϕ177 mm core, calculated using all the measurement data in both profiles A and B, is about 5780 m/s. This can be taken as an approximation to the P wave velocity of the undamaged host rock. Pettitt et al. (2001) obtained a value of 5900 m/s in their *in situ* ultrasonic

measurements in the Prototype Repository area at Äspö HRL. The *in situ* measurements in the TBM tunnel by Falls and Young (1996) and Olsson et al. (1996) showed that the P-wave velocity of the Äspö rock was in the order of 5900-6000 m/s. It is seen that the P-wave velocity measured in the ϕ177 mm core is slightly lower than that measured *in situ*.

The difference of the overall average P-wave velocity between the ϕ45 mm core and the ϕ177 mm core may be a quantitative indicator how serious the ϕ45 mm core has been damaged. The overall average P-wave velocity of the ϕ45 mm core specimens is about 5550 m/s. The reduction in the P-wave velocity compared to that measured on the ϕ177 mm core is about (5780-5550) = 230 m/s, i.e. about 4% of the P-wave velocity of the host rock.

The maximum error for the calculated P-wave velocity in the 45 mm core specimens is estimated at ± 40 m/s. The corresponding error for the measurements on the 177 mm cores is ± 4 m/s.

5.4 Thin-section analyses of sample disturbance

The results of the thin section work showed that the mapped fractures are primarily radial (parallel to core axis) and that they diminish in number when moving towards the interior of the core. The background frequency of micro-cracks in approximately 1 fracture/mm in the interior of the studied 177 mm core, whereas the frequency in the outer 3 mm is in the order of 1.7-3.3 fractures/mm (Li, 2001), cf. Figure 5-5.

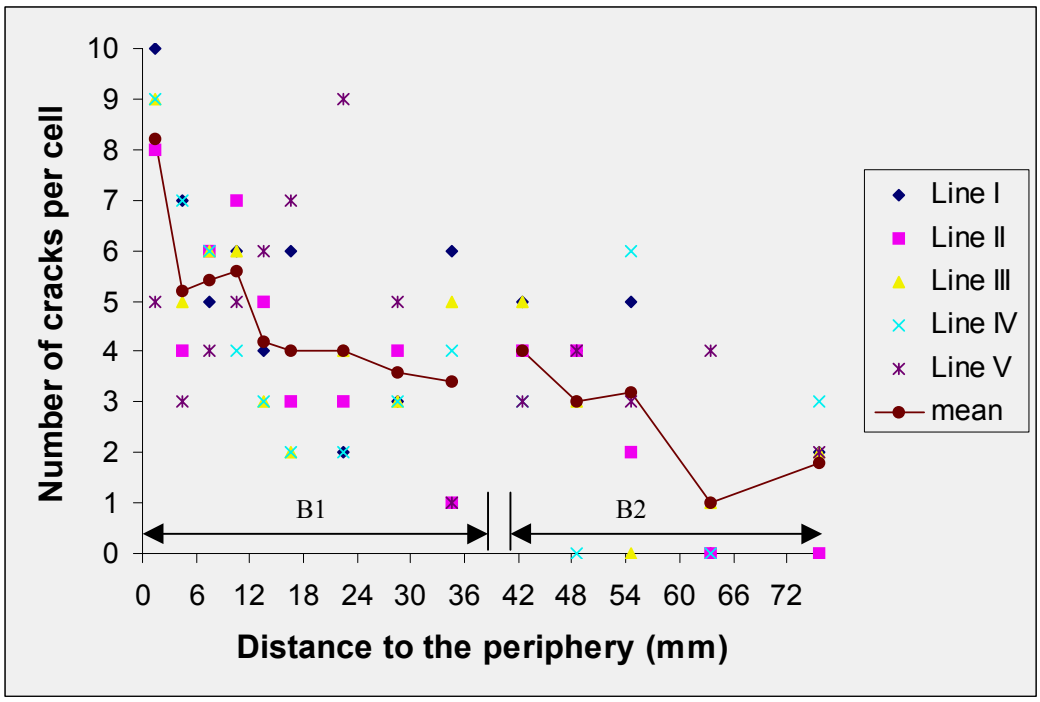

Figure 5-5. *Number of fractures/cell in samples B1 and B2 vs. distance of the measurement cell to the periphery of the 177 mm core (cell size = 3 mm).*

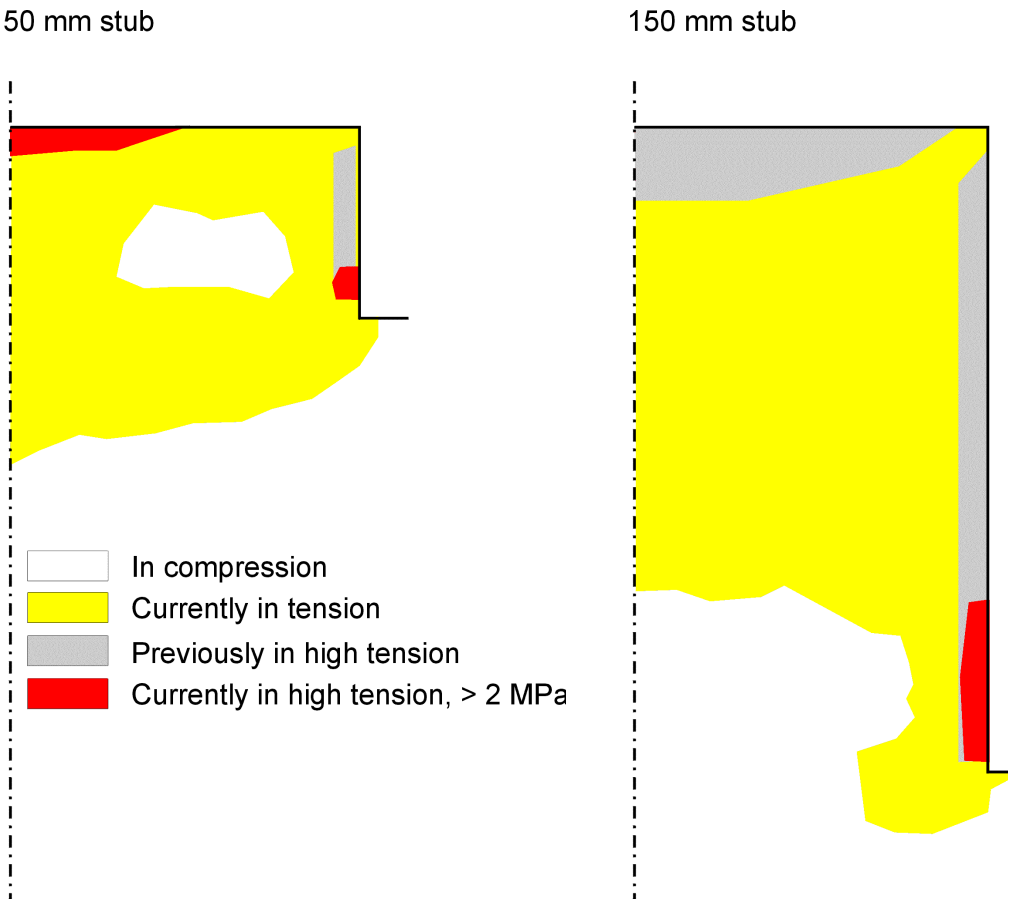

Figure 5-6. *Qualitative illustration of results of axi-symmetrical analysis of the stress situation for a) a 50 mm core stub and b) a 150 mm core stub. Yellow, grey and red areas show areas in tension.*

5.5 Numerical analysis of stress situation

In addition, existing (Hakala, 1999) and new experiment-specific rock mechanical modelling results have been used to assess the effects of drilling and stress relaxation on the core stub and its environment. Figure 5-6 shows the site specific situation both for 50 mm and 150 mm core stubs. The results, in both cases, show large volumes of rock subject to tension, and hence widening of existing micro fractures.

5.6 Usage of core stub for experimental purposes

The effect of the unloading in the relatively low-stressed rock at Äspö is expected to be small, the effects in terms of opening of grain boundaries and widening of existing micro fractures is expected to be minimal. Notwithstanding, the effect is there and has effectively lead to discarding the idea of using the core stub for *in situ* estimation of diffusivity.

Given that the stub is mechanically disturbed plus the possibility that diffusion of weakly sorbing species through the stub may not reach the intact rock beyond the core root, analysis of alternative concepts were performed. The concept eventually put forward was one where the intact rock is accessed using a small diameter borehole through the centre of the core stub as described in previous sections.

6 Discussion and conclusions

The present report reviews the results related to the pilot borehole KA3065A02 and presents results of the telescoped 300/196.5/36 experimental borehole. The drilling of the experimental borehole KA3065A03 was performed with a strong element of interactivity of various logging activities, tentative geological mapping and computerised structural modelling. The objective being to terminate the borehole at the pre-designated depth. Due to problems with poor visibility (borehole TV/BIPS) in combination with material falling out of the core barrel, termination of the borehole at the desired depth relative to the marker main structure (as identified in the pilot borehole) was not possible to achieve. As a result, the produced "core stub" in the borehole is approximately 160 mm long, compared to the originally desired 50 mm.[2]

The longer than wanted stub is not deemed to be a problem for designing and manufacturing the PEEK/Polyurethane packer which will seal off the exposed fracture plane. From an experimental standpoint, the longer stub length will imply that the less sorbing tracers will migrate in a longer section which may show enhanced diffusivity, either due to poor sealing against the packer or due to enhanced diffusivity along the mantel surface of the stub. Assessments of the extent of excavation damage in the stub are underway using micro-seismic techniques in combination with thin section analysis, using core material both from the pilot and experimental boreholes.

The surface relief and detailed geology in the vicinity of the stub has been monitored with video cameras mounted on remote-controlled vehicles and rods, BIPS, endoscope video imaging in the annular slot, manual geodetic surveying and surveying using a total station. These assessments have been supplemented with plaster casting (in a latex liner) of the stub surface. Geologically, the surface of the stub is heterogeneous with variable coverage of calcite, chlorite and altered Ävrö granite (Andersson et al., 2002). From microscopy of the stub surface it is obvious that the mineralogy is complex with variable amounts of quartz, fluorite, chalcopyrite and baryte, low temperature K-feldspar and epidote and mentioned calcite and chlorite.

Discrepancies in orientation of measured fractures correlated between the pilot and experimental boreholes are attributed to the small distance between the boreholes in combination with the small diameter of the pilot borehole. The same type of discrepancy between projected and physically observed fractures is also noted for the 36 mm. In this case, the discrepancy may be attributed to orientations of fractures being obtained exclusively by core mapping on the small diameter core (22 mm). It should also be kept in mind that also very minute fractures have been included in the documentation of these boreholes and these may have a limited extent (possibly terminating between the boreholes). As a result of the mineralogical study of the structures in the 36 mm part of the borehole it is suggested that some of these fractures can be grouped together to form larger structures, that in turn may be easier to extrapolate between the boreholes.

7 References

Andersson P., Byegård J., Dershowitz, W. Doe T., Hermanson J., Meier P., Tullborg E-L., Winberg A., 2002a. TRUE Block Scale Project. Final report. 1. Characterisation and model development. Swedish Nuclear Fuel and Waste Management Company. SKB Technical Report TR-02-13.

Byegård, J., Johansson, H., Andersson, P., Hansson, K. and Winberg, A. 1999. Test Plan for the Long-Term Diffusion Experiment. Swedish Nucelar Fuel and Waste Management Company. Äspö Hard Rock Laboratory. Progress Report HRL-96-01.

Falls, S.D. and Young, R.P., 1996. Examination of the excavation disturbed zone in the Swedish ZEDEX tunnel using acoustic emission and ultrasonic velocity measurements. In Proc. of EUROCK'96, pp. 1337-1344, Turin, Italy, 1996.

Hakala, M. 1999. Numerical study on core damage and interpretation of in situ state of stress. Posiva Technical Report 99-25. ISBN 951-652-080-4.

Li, Y. 1997. Drilling-induced core damage and its relationsjip to crustal in situ state of stress and rock properties. PhD Thesis, U. of Alberta, Edmonton, Alberta.

Olsson, O. et al., 1996. ZEDEX - A study of the zone of excavation disturbance for blasted and bored tunnels. Swedish Nuclear Fuel and Waste Manahgement Company, SKB Äspö Hard Rock Laboratory, International Cooperation Report ICR-96-03.

Pettitt, W., Baker, C. and Young R.P., 2001. Acoustic emission and ultrasonic monitoring during the excavation of deposition holes in the Prototype Repository. Swedish Nuclear Fuel and Waste Manahgement Company, SKB Äspö Hard Rock Laboratory, International Progress Report IPR-01-01.

Winberg, A., Andersson, P., Hermanson, J., Byegård, J., Cvetkovic, V. and L. Birgersson 2000. Final report of the first stage of the tracer retention understanding experiments. Swedish Nuclear Fuel and Waste Management Company (SKB), Technical Report TR-00-07. ISSN 1404-0344.